Geol. Mag. **155** (*1*), *2018, pp. 1–19.* © *Cambridge University Press 2016*
doi:10.1017/S0016756815001132

Iron and silica enrichments in the middle Albian neptunian dykes from the High-Tatric Unit, Central Western Carpathians: an indication of hydrothermal activity for an extensional tectonic regime

KRZYSZTOF BĄK*†, JOANNA KOWALCZYK‡, ANNA WOLSKA*, MARTA BĄK‡ & LUCYNA NATKANIEC-NOWAK‡

*Faculty of Geography and Biology, Pedagogical University of Cracow, Podchorążych 2, 30–084 Kraków, Poland
‡Faculty of Geology, Geophysics and Environmental Protection, AGH University of Science and Technology, Mickiewicza 30, 30–059 Kraków, Poland

(*Received* 20 July 2015; *accepted* 29 December 2015; *first published online* 3 March 2016)

Abstract – Studies dealing with the response of subaqueous volcanic and hydrothermal activities to carbonate sedimentation in hemipelagic environments affected by tectonic processes are comparatively rare. Here, a microfacies record with combined chemical data from the neptunian dykes found at an intrabasinal ridge (Tatric Ridge; Carpathian domain of the Western Tethys), close to a source of alkaline volcanism with possible hydrothermal vents (Zliechov Basin), is presented. The characteristic features of the neptunian dykes, up to 20 cm thick, in the middle Albian echinoderm-foraminiferal limestones (Tatra Mountains, Inner Carpathians) are their red fillings. Microprobe and x-ray diffraction analyses show that this reddish material, partly mixed with sparitic clasts coming from the host limestone, consists mainly of hematite crystals which are associated with low crystalline silica and quartz. The microfacies data suggest that the reddish infillings of the dykes is partly related to dissolution processes inside the fissures that could have taken place during the transport of $FeCl_3$ fluids together with silica gel. The fluids could have been derived from hydrothermal vents occurring along the extensional faults in the neighbouring Zliechov Basin. Rare Earth element (REE) signatures of the reddish infill (i.e. low values of total REE content, chondrite- and Post-Archean Australian Shale-normalized REE + Y patterns with negative Ce anomaly) and a high Y/Ho ratio suggest authigenic removal of REEs from the water column. This suggests that the fissures were open to the sea bottom and were in contact with sea water during their filling.

Keywords: neptunian dykes, iron and silica enrichments, hydrothermal and hydrogenic sources, extensional regime of basin.

1. Introduction

Shallow-water carbonate platforms with Urgonian-type sedimentation existed in various regions of the Mediterranean Tethys during Early Cretaceous time (e.g. Arnaud-Vanneau *et al*. 1979, 1982; Philip, Masse & Bessais, 1989; Michalík & Soták, 1990; Babinot *et al*. 1991). The sequences of these facies were documented among others from the Western Carpathians, including the Tatric successions (Michalík, 1994). In the latter locality, carbonate platform sedimentation containing biohermal and lagoonal facies took place on the Tatric Ridge (Passendorfer, 1930; Lefeld, 1968, 1974; Michalík & Vašiček, 1989; Michalík & Soták, 1990; Mišik, 1990), an internal part of the Central Western Carpathian region (e.g. Plašienka, 1997, 1999). The palaeomagnetic data (Grabowski, 1997) from the Tatra Mountains indicate their proximity to the European plate at least in the post-early Aptian – early Turonian time span. Since early Aptian, time regional tectonic processes have resulted in the subsequent lowering of this platform below the photic zone (Michalík, 1994); the Urgonian-type benthic organisms (containing rudist and orbitolinids) finally died on the Tatric Ridge during middle Albian time (Masse & Uchman, 1997). Pelagic and hemipelagic carbonate sediments deposited under open marine conditions replaced the shallow-water facies in this area (e.g. Passendorfer, 1930; Lefeld, 1968; Mišik, 1990; Krajewski, 2003). Due to tectonic processes, relief of the carbonate platform was significantly changed during late–middle Albian time. The occurrence of tectonic breccias and neptunian dykes, lying mainly at the top of the Urgonian facies, indicate rapid tectonic processes at that time which caused changes in the palaeogeography of the Tatric Ridge (Krajewski, 2003). Elevated blocks with steep slopes and deep troughs were interpreted for this region on the basis of facies patterns and large differences in the thickness of underlying Albian carbonate sediments (Krajewski, 1981). In such troughs, the relatively quick sedimentation of carbonate material was interrupted by subsequent tectonic movements (earthquakes), which is exemplified by an occurrence of younger neptunian dykes inside of lower–middle Albian

†Author for correspondence: sgbak@cyf-kr.edu.pl

echinoderm limestones in such settings (Krajewski, 2003).

The characteristic feature of the neptunian dykes in the lower Albian Tatric sequences is their red colouration, related to the occurrence of iron oxides. According to Krajewski (2003), many of them are filled with recrystallization products of the original land-derived iron hydroxides, formed during the emergence and karstification of the Tatric Ridge. As a consequence, the sediment in the dykes contains washed-out karstic residuum incorporated into marine limestone. In addition to the brecciated horizons with neptunian dykes lying at the base of the carbonate open-marine succession, there were also younger brecciated horizons with neptunian dykes red to pinkish in colour. They were found in thick successions of white echinodermal-foraminiferal limestone, which infilled the submarine trough. The sediment in these dykes is enriched with iron oxides and there is also crystal of quartz inside. The origin of these infillings remains unknown. The aim of this study is to elucidate the source of the iron and silica enrichments in this type of neptunian dyke. We hypothesized that these enrichments could be related to hypergenic marine processes at the basin floor (weathering in marine environment). Nonetheless, hydrothermal sources of iron and silica cannot be excluded here, due to an occurrence of ocean-floor alteration processes at and near the Tatric Ridge (Hovorka & Spišiak, 1988; Spišiak *et al.* 1991; Spišiak & Balogh, 2002; Madzin, Sýkora & Soták, 2014).

2. Geological setting

The Tatra Mountains belong to the Tatric unit (Tatricum), one of the major units of the Central Western Carpathians (Fig. 1a; Passendorfer, 1930; Andrusov, 1968; Plašienka, 1997, 1999). They consist of a pre-Alpine crystalline basement composed of Variscan metamorphic rocks and granites, overlain by sedimentary cover sequences and nappes. The sedimentary cover is of ?Permian – Late Cretaceous age, with a total thickness of up to 2000 m (Nemčok *et al.* 1993). It consists of sedimentary sequences deposited on the crystalline basement and overthrusted sediments (nappes) originating from marginal marine environments (e.g. Rabowski, 1959; Kotański, 1961; Passendorfer, 1978).

The Lower Cretaceous sediments, deposited directly on the crystalline basement of the Tatric Ridge, consist of the Urgonian platform limestones and related slope sediments (e.g. Passendorfer, 1930; Morycowa & Lefeld, 1966; Lefeld, 1968, 1974; Michalík & Vašiček, 1989; Michalík & Soták, 1990; Masse & Uchman, 1997). In the western part of this area, a few small lenticular bodies and bands (2–30 m thick) of alkaline volcanic rocks classified as hyalobasanites occur (Kotański & Radwański, 1959; Hovorka & Spišiak, 1981; Spišiak & Hovorka, 1997; Hovorka, Dostál & Spišiak, 1999; Ivan, Hovorka & Méres, 1999; Staniszewska & Ciborowski, 2000). They are sandwiched with carbonate breccia containing calpionellid microfaunas, whose stratigraphic position corresponds at the latest to the Tithonian through the ?early Valanginian (Madzin, Sýkora & Soták, 2014). These shallow-water Urgonian-type carbonate sediments (locally with volcanic rocks) partially emerged during late Aptian – early Albian time. They were subsequently covered by the Albian basal sandstone bed or breccia and overlain with dyke infillings by fossiliferous phosphate- and glauconite-rich limestone, passing into upper Albian – Cenomanian marlstone and a rhythmic marlstone-siltstone-sandstone sequence (Zabijak Formation; Krajewski, 2003; Bąk & Bąk, 2013). The brecciated zone containing the neptunian dykes, classified as the Ku Stawku Bed of the Zabijak Formation (Fig. 1e; Krajewski, 2003), lies within the light grey limestones (Żeleźniak Member) *c.* 3 m above the top of the light grey organodetrital limestones (Wysoka Turnia Limestone Formation; Lefeld, 1968, 1985) of Aptian – middle Albian age (Masse & Uchman, 1997).

3. Materials and methods

The studied section was found in the abandoned quarry at the Hala Gąsienicowa Alp within the Sucha Woda Valley, which is a part of the High Tatra Mountains (Fig. 1b–d). Twenty-three samples were collected from the brecciated zone containing the neptunian dykes and from the surrounded limestone (Figs 1e, 2a). The standard optical examinations of the transmitted light of the thin and polished sections were carried out under a BA310POL polarizing microscope with photo capture using Panasis software.

Analyses of the main minerals (hematite, quartz, calcite, dolomite) were carried out using a FEI Quanta 200 FEG scanning electron microscope (SEM), equipped with an energy-dispersive (EDS) detector and a Hitachi-S 4700 SEM with a Voyager 3100 EDS spectrometer (NORAN). In both cases, the time of analysis was 100 s for each point and the resolution was 1.5 nm. The data were corrected using the ZAF/PB program. The SEM observations and EDS analyses were made in the Scanning Electron Microscopy Laboratory at the AGH University of Science and Technology and at the Institute of Geological Sciences at Jagiellonian University.

The mineral composition of the red-coloured sediment infilling the dykes was determined by X-ray diffraction (XRD) analysis at the Institute of Geological Science, Jagiellonian University. These analyses were conducted on a Philips X'Pert diffractometer with the PW 1870 generator and the PW 3020 vertical goniometer, using filtered CuKα radiation. The instrument settings were electric potential U 40 kV, current I 30 mA, a scanning speed of 1°/min and a chart speed of 10 mm/min.

Three samples of sediment (containing a little admixture of surrounding rock) and one sample from the surrounding unaltered limestone were analysed for major and minor element concentrations at the Bureau Veritas Minerals Laboratories, Vancouver, Canada.

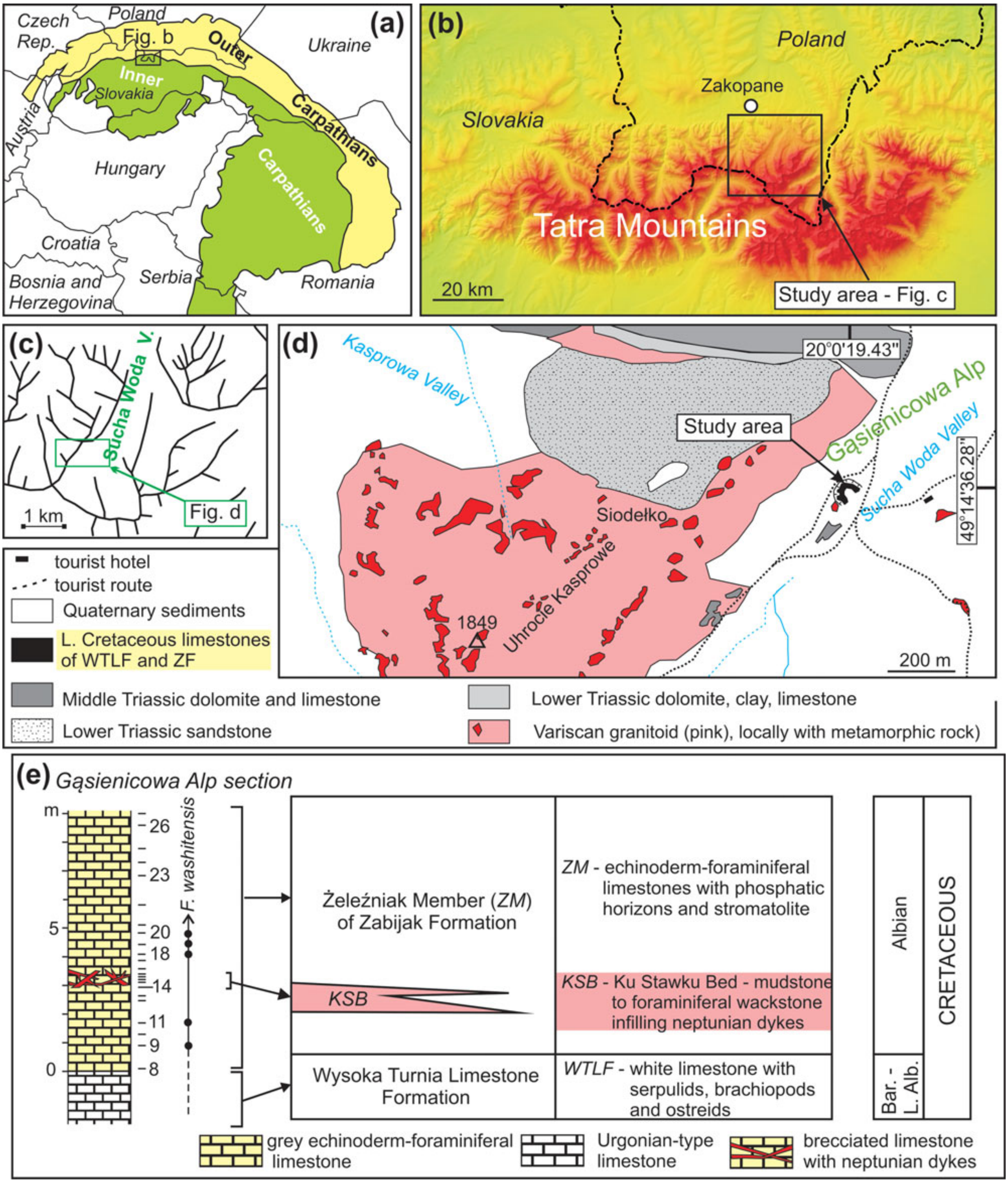

Figure 1. (Colour online) (a) Simplified geological map of the Carpathians. (b, c) Location of the Sucha Woda Valley in the Tatra Mountains (Inner Carpathians) (contour map after Bryndal, 2014). (d) Geological map of the study area (map after Guzik & Jaczynowska, 1978). WTLF – Wysoka Turnia Limestone Formation; ZB – Zabijak Formation. GPS data based on EPSG: 2180. (e) Barremian–Albian lithostratigraphic scheme and lithologic log of the section studied (lithostratigraphy after Krajewski, 2003; occurrence of *Favusella washitensis* Carsey, this study).

Total abundances of the major oxides, several minor elements, rare Earth and refractory elements were analysed by inductively coupled plasma (ICP) emission spectrometry, following lithium metaborate/tetraborate fusion and dilute nitric acid digestion. Loss on ignition (LOI) was determined by the weight difference after ignition at 1000°C for >2 h. Moreover, separate 0.5 g samples were digested in Aqua Regia and analysed by ICP mass spectrometry to determine the precious and base metals. The detection limits ranged from 0.002 wt% to 0.01 wt% for major oxides, from 0.1 ppm to 20 ppm for trace elements and

https://doi.org/10.1017/S0016756815001132 Published online by Cambridge University Press

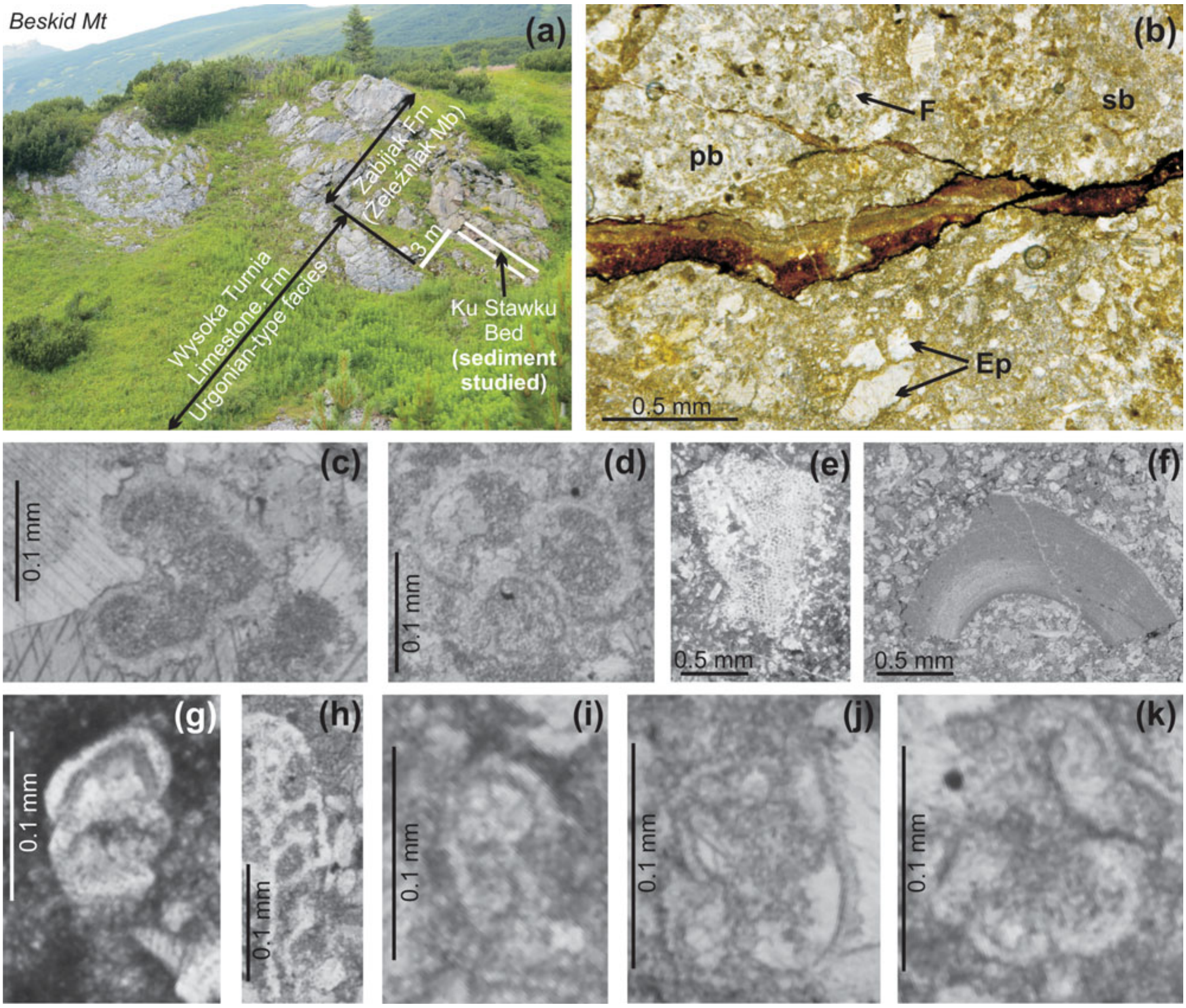

Figure 2. (Colour online) (a) Photograph of the abandoned quarry at Hala Gąsienicowa Alp (Sucha Woda Valley, Tatra Mountains) with location of the sediments studied. (b) Echinoderm-foraminiferal packed biomicrite (pb) and sparse biomicrite (sb) as typical microfacies of the host sediment containing neptunian dykes, consisting of echinoderm plates with jagged edges after dissolution and/or recrystallization (Ep) and benthic foraminiferal test (F); small neptunian dyke enriched in iron oxides (central part of photomicrograph). (c, d) *Favusella washitensis* Carsey, stratigraphically important planktonic foraminiferal species from the host limestone: (c) HGas-9; (d) HGas-11. (e–k) Microfossils in echinoderm-foraminiferal biomicrites: (e) fragment of echinoderm plate; (f) fragment of rudist shell; (g, h) benthic foraminifers ((g) ?*Dentalina* sp.; (h) ?*Nodosaria* sp.) as a residue clast partly surrounded by reddish filling from the micro-dyke; (i–k) planktonic foraminifers from genus *Hedbergella*. All photomicrographs from sample HGas-15b.

from 0.01 ppm to 0.1 ppm for the rare Earth elements. The CANMET- and USGS-certified reference materials were used as monitors of data quality.

4. Results

4.a. Microfacies and age of the host rock

The sediments studied macroscopically contained a sequence of monotonous, poorly laminated, grey limestones and consisted of two types of microfacies: packed biomicrite passing to sparse biomicrite (Fig. 2b). Allochem content varied from 30 % up to 70 % in the thin-sections under view. They were mainly disarticulate, fragmented echinoderm skeletons, 50–200 µm across (Fig. 2e), which represent various types of singular, porous plates belonging predominantly to holothurids, asteroids and echinoids. Most of the plates possessed jagged edges revealing evidence of dissolution and later recrystallization (Fig. 2b). Additionally, the limestone consisted of benthic and planktonic foraminifers (Fig. 2b, g–k), fragments of rudist shales (Fig. 2f) and clasts of Lower Cretaceous organodetrical limestones.

The microfacies studies showed that among the planktonic foraminiferal assemblages, only *Favusella washitensis* Carsey (Fig. 2c, d) was a stratigraphically important species that could help determine the position of the studied limestones containing neptunian dykes. This species was found in the limestone succession below and above the horizon with dykes (Fig. 1e). Its stratigraphic range was discussed by Rösier, Lutze & Pflaumann (1979) and confirmed by Caron (1985) and

https://doi.org/10.1017/S0016756815001132 Published online by Cambridge University Press

Koutsoukos, Leary & Hart (1989) as of lower Albian (*Ticinella primula* Zone) through middle Cenomanian (*Rotalipora reicheli* Zone); however, its detection in lower Albian deposits is restricted to epicontinental seas (Risch, 1971; Michael, 1972; Ascoli, 1976; Koutsoukos, Leary & Hart, 1989). In the same locality (Wysoka Turnia Limestone Formation; compare Fig. 1), this species was noticed by Masse & Uchman (1997) in an upper part of the Urgonian-type facies. On the other hand, planktonic assemblages do not include keeled taxa (*Pseudothalmanninella* and *Parathalmanninella*) which are known to have appeared during late Albian time (e.g. Gale *et al*. 2011). All of these data may suggest that the sediments containing neptunian dykes are of middle Albian age.

4.b. Description of the neptunian dykes

The dykes were found in the brecciated part of the limestone, showing various shapes and sizes (Fig. 3). Most of them were connected to each other and filled with the same type of sediment, including mainly red infill (Fig. 3a–f). Some of them contained internal breccia (Fig. 3d). In cross-sections, most of the dykes were a few centimetres thick; locally, the thickest parts were up to 20 cm. Silica encrustation of a few centimetres thickness has been observed in the wider parts of the dykes (Fig. 3g). The orientation of the dykes varied due to numerous branches which rapidly thinned out in various directions; however, the thickest dykes were generally vertical. The walls appeared to be sharp when viewed macroscopically and were covered by ferruginous encrustations and/or calcite cements (Fig. 3a–d).

Study of the microfacies showed that the limestones also contained several generations of cross-cutting microchannels (Fig. 4a, b) from less than several micrometres up to several millimetres in width, which were usually secondarily filled in by calcite spar (CS). Two sets of such channels, which crossed at least two previously formed generations of channels filled with CS, were unique because they were partially or completely filled with red, opaque, microcrystalline material (RS) (Fig. 4a, b). These channels continued from main dykes and were filled with red material; they were visible in outcrop walls and were observed branching through the host limestones even on the microscopic scale. The red-filled channels (RS) cut host biomicrites as well as previous channels filled in by calcite (CS), and they were cut by subsequent generations of channels also filled with calcite (CS). The spatial and temporal relations between the CS and RS were clearly visible as the systems of channels intersected at a sharp angle. However, in some cases the RS and CS appeared to have developed perpendicularly as CS inside RS or CS next to RS (Fig. 4d–f).

4.c. Petrography of host rock

From a petrographic point of view echinoderm-foraminiferal packed biomicrite, which is typical of the microfacies of the host limestone, consisted of calcite crystals, skeletal debris and rare crystals of hematite. The dimensions of the carbonate particles ranged from less than 25 μm to 2 mm. Rounded low crystalline silica and microcrystalline quartz concentrations (up to 2 mm) were also found in the biomicrites (Fig. 5a, b). Their brown colouration was due to the occurrence of scattered hematite crystals (Fig. 5a, c), which were also found along the straight fractures (Fig. 5).

4.d. Texture and petrography of infilling material

There were two types of micro-dyke fillings. The first type contained almost pure, homogeneous, opaque reddish material which filled the micro-space of the dykes completely (Fig. 4d). The second type comprised reddish, opaque material similar to that of the first type but mixed with rounded sparitic clasts (Fig. 4c), which in some cases were gravitationally segregated. The clasts displayed the same features as the sparitic components of the host limestone. These included corroded and/or regenerated echinoderm plates, partly with their original porosity, rare calcareous benthic foraminifers and pithonellids. In the widest micro-dykes, the sparitic clasts were situated close to the walls of the dyke (Fig. 4g). Others were filled with internal breccia, where host-rock fragments constituted a more than 50 % of the primary caverns and the reddish opaque material was the main matrix (Fig. 4g–i). Microprobe analyses of the reddish material from the dykes indicated a predominant occurrence of hematite (Table 1). They were detected in crystalline thin plates, which were densely packed and may have entirely filled the dyke or encircle the quartz and calcite grains (Fig. 6a). Locally, densely packed hematite crystals formed clearly visible lamination, intercalating laminae with clasts coming from the host rock (Fig. 6b). The hematite microcrystals exhibited trigonal symmetry, and their sizes ranged from 0.5 to 1.0 μm (Fig. 6c).

EDS analysis of the crystals and clasts from the internal breccia, which were surrounded by the reddish, hematite-bearing matrix, enabled the detection of calcite, quartz and dolomite inside (Table 2). The calcite crystals (up to 10 μm) were strongly corroded, with several sharp-edged caverns (Fig. 6e). The sizes of the individual quartz crystals were 1–10 μm (Fig. 6a). The associated dolomite crystals (Fig. 6d) had similar dimensions to the quartz crystals (up to 10 μm).

4.e. XRD analysis of infilling material

XRD of the reddish filling confirmed the microscopic observations and EDS analysis. Based on the XRD patterns of samples (HGas 13, 14 and 15a), the presence of hematite, calcite, quartz and dolomite were verified (Table 3; Fig. 7). Hematite was recognized based on the appearance of following d(hkl) characteristic for α-hematite (diffraction data for α-hematite 06–0502): 2.69 Å (I = 100), 2.51 Å (I = 80), 1.691 Å (I = 80), 3.68 Å (I = 70), 1.837 Å (I = 70), 1.484 Å (I = 70).

Table 1. Microprobe chemical analyses of reddish infill of the neptunian dykes (sample HGas-15a). Numbers of cations (ions) calculated on the basis of 6 (O); CO_2 has not been determined.

Points	Fe_2O_3	V_2O_3	Al_2O_3	SiO_2	CaO	MgO	P_2O_5	K_2O	
9a	76.15	–	4.42	8.08	4.97	2.36	3.86	0.16	
10a	78.92	–	4.85	9.15	3.31	1.95	1.82	–	
12a	81.48	–	4.99	5.94	4.43	2.34	0.82	–	
18a	84.14	0.15	4.91	7.23	1.13	1.93	0.52	–	
19a	84.32	–	4.22	9.14	0.74	1.58	–	–	
20a	97.33	–	0.98	0.90	0.79	–	–	–	
Points	Fe^{3+}	V^{5+}	P^{5+}	Al	Si	Ca	Mg	K	Sum
9a	1.353	–	0.077	0.123	0.191	0.126	0.083	0.005	1.958
10a	1.411	–	0.037	0.136	0.217	0.084	0.069	–	1.954
12a	1.500	–	0.017	0.144	0.145	0.116	0.085	–	2.008
18a	1.538	0.002	0.011	0.140	0.176	0.029	0.070	–	1.966
19a	1.534	–	–	0.120	0.221	0.019	0.057	–	1.952
20a	1.923	–	–	0.030	0.024	0.022	–	–	1.999

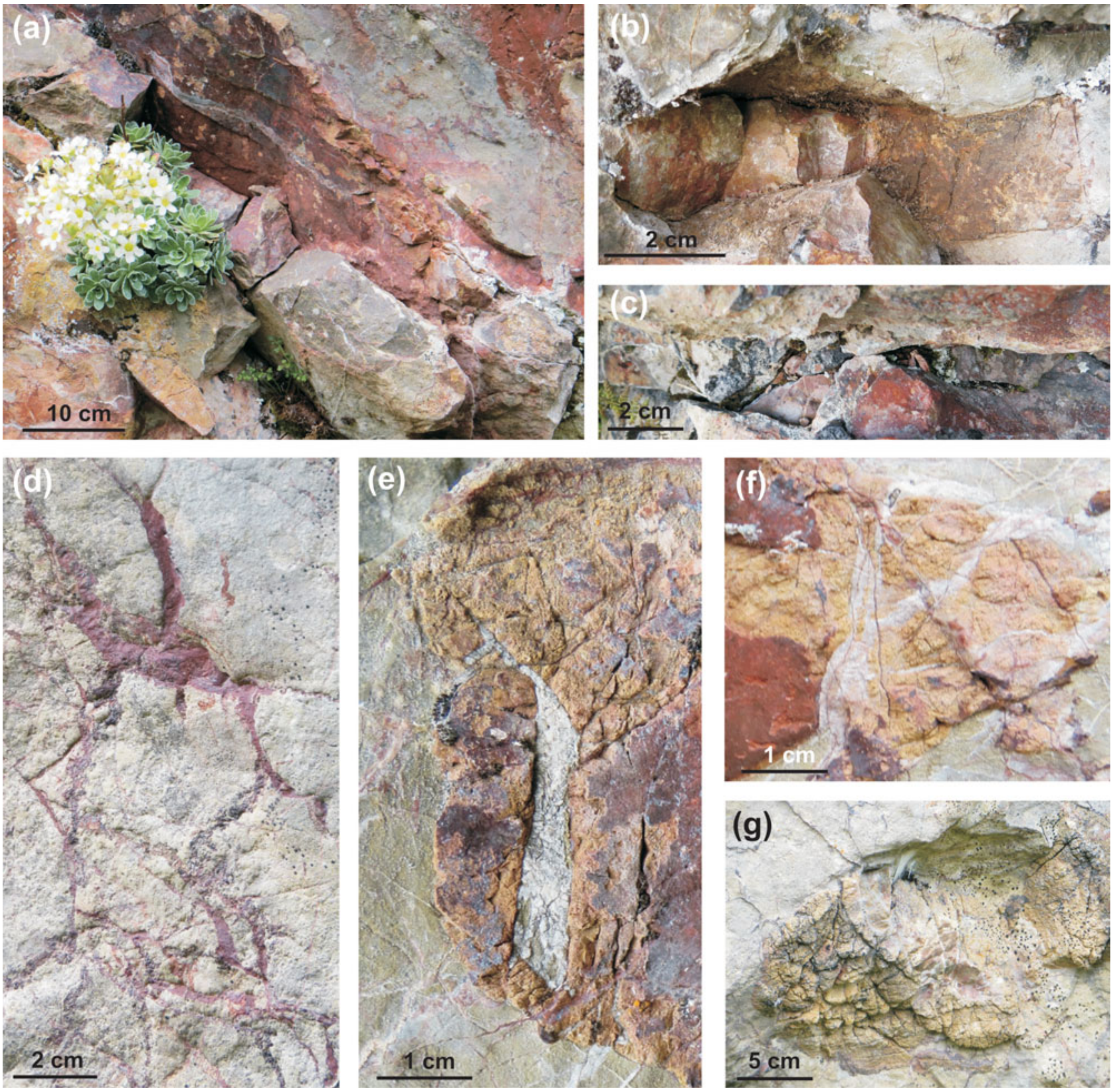

Figure 3. (Colour online) Photographs of neptunian dykes in the Albian limestones at the Gąsienicowa Alp section, Sucha Woda Valley, Tatra Mountains. (a–f) Dykes with iron oxide encrustations; (f) shows iron oxide dykes which are crossed by another system of dykes filled with calcite. (g) Silica encrustation inside of wider part of the dyke.

https://doi.org/10.1017/S0016756815001132 Published online by Cambridge University Press

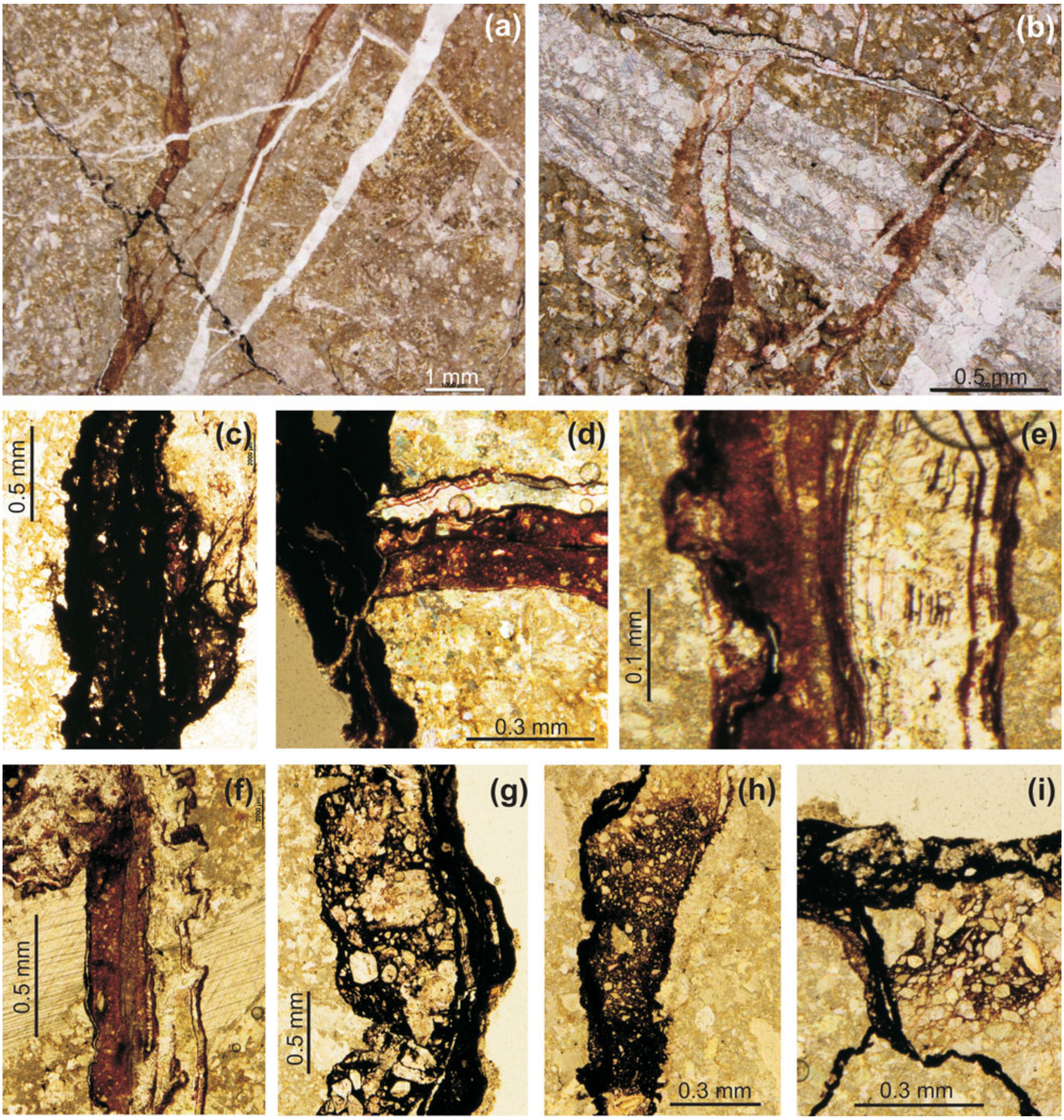

Figure 4. (Colour online) (a) Two generations of channels filled with red opaque microcrystalline material (RS1, RS2) and two generations of channels filled with calcite spar (CS1, CS2) developed in sparse biomicrite. (b) Cross-cutting of two generations of channels filled with calcite spar (CS1, CS2). This system was crossed by channels filled with Fe encrustations (RS), which were partly secondarily filled with calcite. Texture of neptunian dykes containing Fe-bearing minerals (dark brown) which filled the dykes: (c, d) almost completely, (e, f) partially, containing residue after dissolution of host limestone where elements containing sparite left after this process, or (g, h) as rounded material left after stepwise dissolution of sparitic clasts derived from host limestone or (i) micro-dykes opened by stepwise leaching of micrite in host rock with sparitic bioclasts, which might have formed after the internal breccia.

The strong peak signals are typical of well-crystallized quartz (diffraction data for quartz 03–0444). The presence of calcite was established on the basis of the following diffraction peaks: 3.03 Å, 3.852 Å, 1.8726 Å, 2.094 Å. Finally, a minor phase of dolomite (2.90 Å, $I = 100$) was confirmed on the basis of its strongest diffraction peak. The proportion of hematite to calcite varied between the samples studied, which is related to the various types of dyke fillings visible in the thin-sections.

4.f. Geochemistry of infilling material

All samples representing the neptunian dykes together with the host rock from the immediate vicinity displayed a high content of CaO and various admixtures of

https://doi.org/10.1017/S0016756815001132 Published online by Cambridge University Press

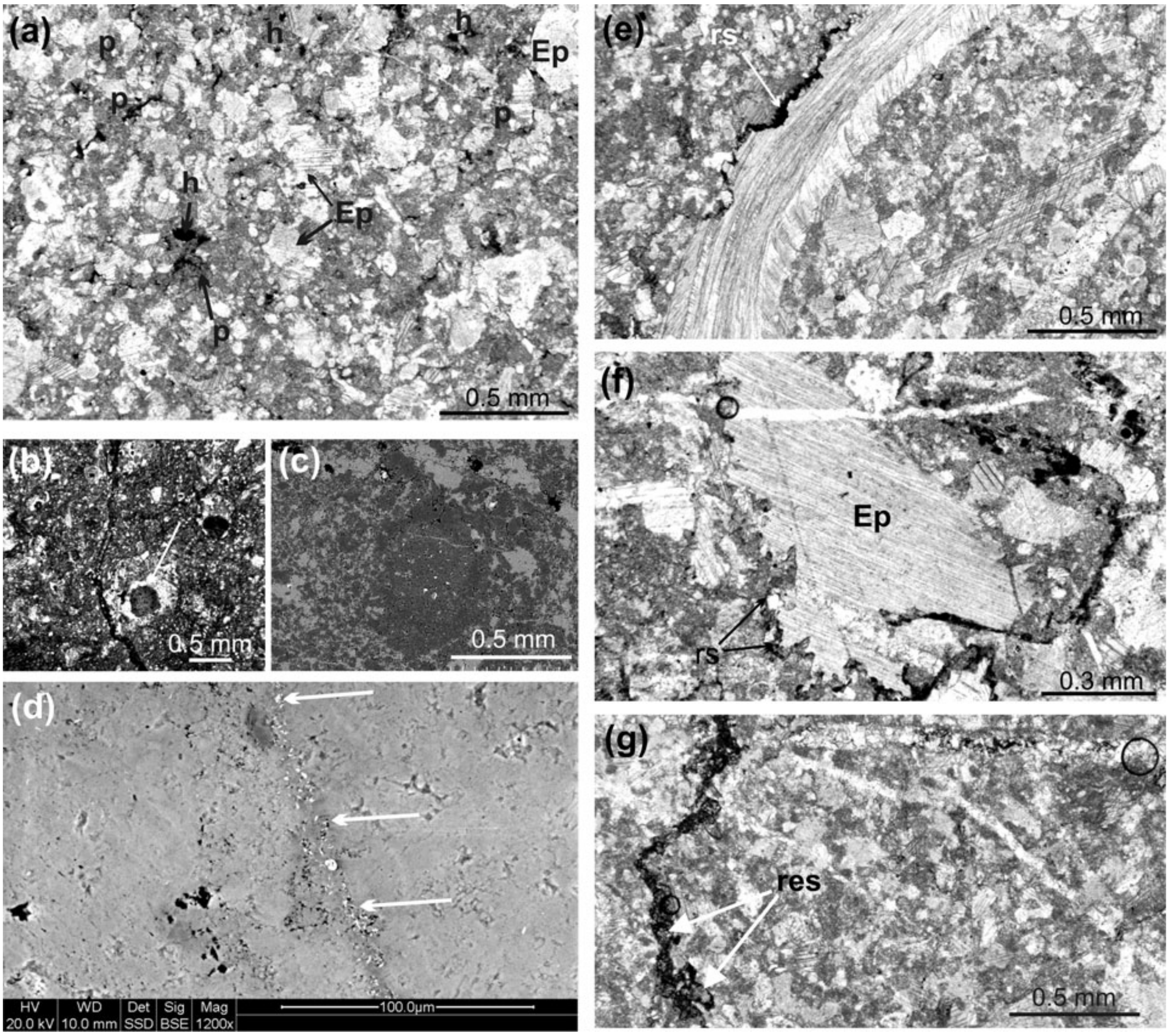

Figure 5. (a) Phosphates (p), hematite (h) and echinoderm plates (Ep) in packed biomicrite. (b, c) Rounded low crystalline silica containing scattered hematite. (d) Hematite microplates (arrows) arranged along the straight fracture (backscattered electron image). (e) The thinnest infillings visible as reddish seams (ferric oxyhydroxides; rs) bordering fragments of bivalve shells, which usually consist of calcite spare (HGas-13). (f) Reddish seams in place of contact of calcitic bioclast (echinoderm plate; Ep) with micrite (HGas-14). (g) Seams opened further (expanded) by replacing (leaching) micrite from the host limestone; more resistant calcitized or sparitic particles left as residue (res) (HGas-13).

major elements (SiO_2, Fe_2O_3, Al_2O_3, MgO, P_2O_5), trace elements (Sr, V, Cu, Ni, Zn, Co, As) and rare Earth elements or REE + Y (Table 4). There were small differences in the chemical compositions of the filling of the neptunian dykes (samples HGas-13, 14 and 15a) and the host rock (sample HGas-15c). The reddish filling was depleted in P_2O_5 (value lower by *c.* 60 %), Co (by 50 %), Ni (by 60 %), Sr (by 10–20 %), V (by 40 %), Zr (by 30 %), Cu (by 75 %), Zn (by 30 %), As (by 50 %) and REE (by 20–40 %).

The ΣREE content in the host rock was higher than in the dykes (by 20–40 %). The chondrite- and PAAS-normalized REE + Y patterns were similar between the dykes and the host rock, emphasized by Ce negative anomaly with Gd and Y positive anomalies (Table 5). All of the materials studied exhibited super chondritic Y/Ho ratios (38–46.7) near to the values of seawater (44–74; Bau, 1996). The Ce/Ce∗ values (0.29–0.34) were similar to oceanic water values, which range from <0.1 to 0.4 (Elderfield & Greaves, 1982; Piepgras & Jacobsen, 1992).

5. Discussion

5.a. Spatial relation between dykes and host rock

Taking into account the pattern of the dykes, their dimensions and the composition of the clasts, it should be stressed that the dykes visible in the outcrop at Hala Gąsienicowa Alp represent the internal system of the underwater fissures formed in lithified limestone (Fig. 8a). The fissures were infilled with local carbonate material, crystals of quartz, and were impregnated by iron oxides, silica and calcite cement (Figs 3–6). The total vertical dimensions of the dykes are unknown due to a lack of open initial parts. Fracturing was induced

https://doi.org/10.1017/S0016756815001132 Published online by Cambridge University Press

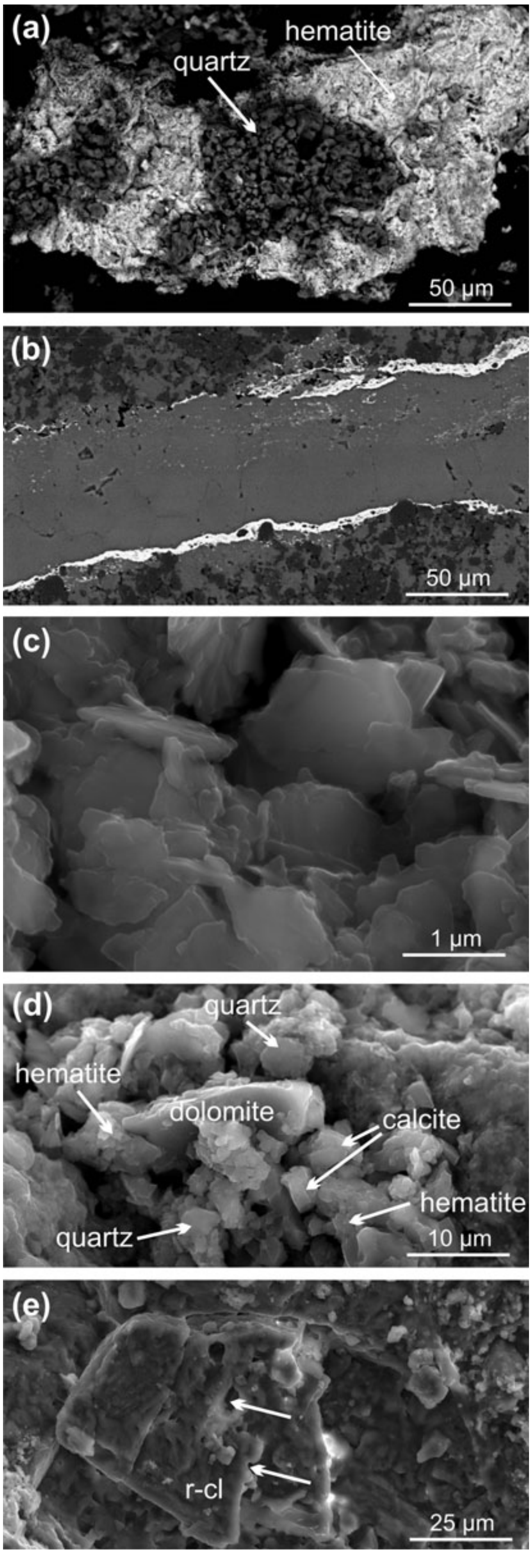

Figure 6. Morphological SEM backscatter and SEM images of components inside the neptunian dykes. (a) Various sizes of quartz (dark grey zones) and hematite crystals (light grey zone) (sample HGas-15a). (b) CS developed inside previous RS visible as iron oxide encrustations on the edge of a dyke (light grey zone) which is filled with calcite (sample HGas-15a). (c) Densely packed plates of hematite (sample HGas-15a). (d) Single crystal of dolomite between calcite, quartz and hematite crystals (sample HGas-15a). (e) Calcite crystal formed by recrystallization of previous echinoderm plate (r-cl) with numerous caverns left from original porosity (arrows) (sample HGas-13).

by extension processes of the platform, which could be responsible for its subsequent lowering.

The microfacies analysis of the reddish fillings in the dykes (i.e. their spatial relation) and shape of the walls show that their origin is partly related to the dissolution process inside the fissures (Figs 4g–i, 8b–e). The thinnest infillings were developed as seams bordering bioclasts, which usually consist of calcite spare, while they were surrounded by micrite (Fig. 5e, f). Reddish (iron oxides) seams started to develop in places where calcitic bioclast contacted with micrite. This shows that fissures can be opened (expanded) by leaching micrite from the host limestone and successively filling them with iron oxides, which are partly associated with quartz crystals (Fig. 8c–e). The more resistant calcitized or sparitic particles were left as residue (Figs 5g, 8e, f); these were usually recrystallized echinoid plates or the calcite infillings of previous channels (Fig. 5f). This interpretation is confirmed by the microsculpture of opposite walls of dykes, which are curved and do not match each other because of the dissolution processes. Additionally, the sparitic clasts are rounded indicating their stepwise dissolution and removal.

5.b. REE signatures of hydrogenic provenance

REE signatures may provide information on the changes in input source flux and oxygenation, thereby elucidating changes related to continental weathering, geochemical evolution, water depth, oceanic circulation and stratification and palaeogeography (e.g. German & Elderfield, 1990; Holser, 1997; Webb & Kamber, 2000; Nothdurft, Webb and Kamber, 2004; Haley, Klinkhammer & Mix, 2005; Piper & Bau, 2013). The data from various types of limestones from Precambrian and Phanerozoic successions (e.g. Bellanca, Masetti & Neri, 1997; Kamber & Webb, 2001; Nothdurft, Webb and Kamber 2004) have been shown to have REE distributions very similar to that of modern Pacific seawater. Original REE signatures with the distinctive characteristics of seawaterxx may therefore be retained in ancient marine limestones.

5.b.1. Source of REEs

Consistent chondrite- and PAAS-normalized REE + Y patterns for the material filling the neptunian dykes and the surrounding limestone (Fig. 9) indicate a similar source for the REEs. This source could generally be influenced by various processes including: (1) authigenic removal of REEs from a water column and early diagenesis (e.g. Sholkovitz, 1988; Koeppenkastrop & De Carlo, 1992; Sholkovitz, Landing & Lewis, 1994; Koschinsky & Hein, 2003; Roberts *et al.* 2012); (2) scavenging processes related to various environmental parameters such as oxygen level, depth and salinity (e.g. Byrne & Kim, 1990; Bertram & Elderfield, 1993); and (3) the addition of terrigenous particles from land, both by fluvial and aeolian transport (e.g. Piper, 1974*a*; McLennan, 1989; Greaves, Elderfield

Table 2. Microprobe chemical analyses of brecciated carbonate material filled the neptunian dyke. Dolomite grain: sample HGas-15a/13a; calcite grains: samples HGas-15a/13b, HGas-14-4, HGas-13-5.

	CaO	MgO	Fe_2O_3	SiO_2	Al_2O_3	MnO	P_2O_5	SrO	
HGas-15a/13a	44.49	30.44	7.42	15.01	1.76	–	0.88	–	
HGas-15a/13b	77.98	1.64	8.29	10.47	1.33	–	–	0.30	
HGas-14-4	93.22	0.55	4.05	0.69	0.65	0.84	–	–	
HGas-13-5	94.15	–	1.67	0.76	0.69	0.54	1.56	0.63	
	Ca	Mg	Fe^{3+}	Si	Al^{3+}	Mn	P^{5+}	Sr	Sum
HGas-15a/13a	2.097	1.996	0.245	0.660	0.091	–	0.033	–	5.122
HGas-15a/13b	4.219	0.123	0.315	0.529	0.079	–	–	0.009	5.274
HGas-14-4	5.522	0.046	0.168	0.038	0.043	0.039	–	–	5.856
HGas-13-5	5.468	–	0.068	0.041	0.044	0.025	0.072	0.026	5.744

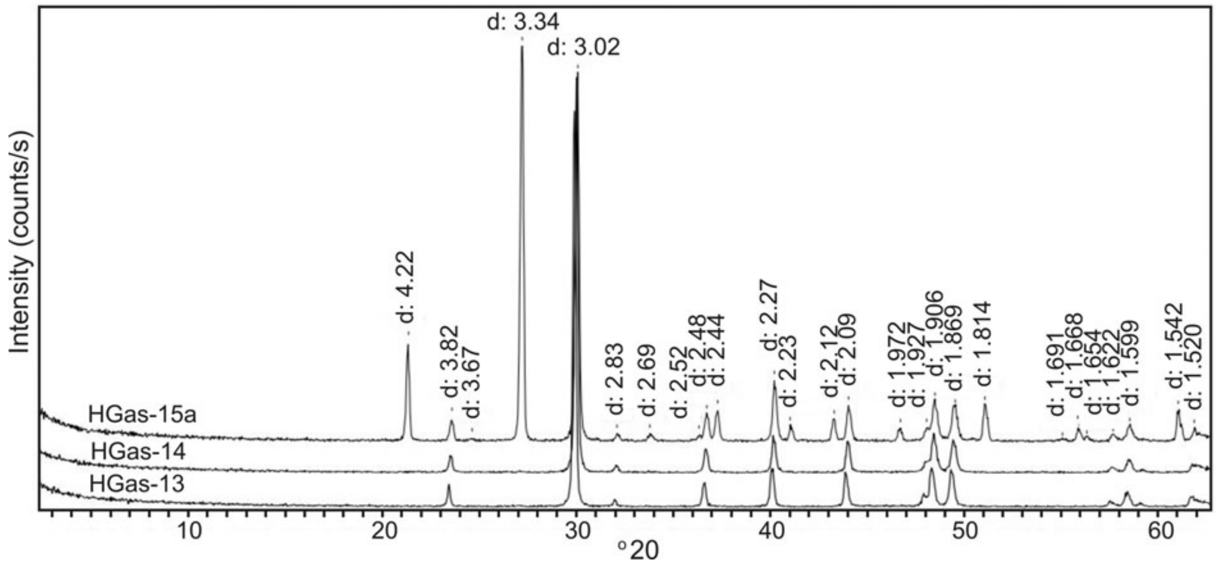

Figure 7. The comparison of XRD patterns of reddish infill from three neptunian dykes.

& Sholkovitz, 1999) and biogenic sedimentation from seawater (e.g. Palmer, 1985; Sholkovitz & Shen, 1995; Reynard, Lécuyer & Grandjean, 1999; Picard *et al.* 2002; Lécuyer, Reynard & Grandjean, 2004; Kocsis, Trueman & Palmer, 2010). Most limestones from various environments have low REE content close to that of normal seawater; this is interpreted as a direct co-precipitation of REEs from seawater with no diagenetic redistribution (e.g. Parekh *et al.* 1977). However, due to contamination by Fe-Mn oxides, phosphates and silicates, their concentration could be higher.

The material from the neptunian dykes under study had a total REE content comparable to that of normal seawater (25–26 ppm; Table 5; e.g. Piepgras & Jacobsen, 1992) or even lower in the case of the Si-enriched dyke (20 ppm). The same conclusion as above is suggested here on the basis of the PAAS-normalized REE patterns of the material from the dykes which were more or less flat, excluding the Y enrichment. This is similar to carbonate and authigenic marine phases, which mainly produced a seawater-like REE pattern (e.g. Piper, 1991; Piper & Bau, 2013). The ΣREE of the host rock was slightly higher (*c.* 20 %; Table 5), which may reflect the contamination of phosphates in the echinoderm-foraminiferal limestone (Table 5) observed in thin-sections of the rock (Fig. 4).

The post-depositional early diagenetic processes related to redox variations may have caused the remobilization and/or fractionation of REEs between the sediment and water (Sholkowitz, Shaw & Schneider, 1992). During REE fractionation, the relative rate of release increases from Lu to La (light REEs > heavy REEs). Similarly, during reoxygenation, removal of dissolved REEs from both the water column and upper pore waters has the same relative rates from light REEs (LREEs) to heavy REEs (HREEs). Such redox changes in the semi-enclosed environment of fractures could be responsible for variations in the relative abundance of LREEs v. HREEs during precipitation of Fe-rich material into the fractures studied.

5.b.2. Ce anomaly

The characteristic feature of the REE curve is a negative Ce anomaly relative to La and Pr when carbonate minerals precipitate in equilibrium with seawater (e.g. Elderfield & Greaves, 1982; De Baar, Bacon & Brewer, 1985; Piepgras & Jacobsen, 1992; Sholkovitz,

https://doi.org/10.1017/S0016756815001132 Published online by Cambridge University Press

Table 3. The bulk X-ray diffraction patterns of reddish infill from three neptunian dykes (A) with a list of the detected phases in the analysed material (B). Data in bold indicate crystalline silica. d_{hkl} is lattice spacing; I is intensity.

A						B				
Sample H-Gas13		Sample H-Gas 14		Sample H-Gas 15a		ICPDS (1997) diffraction data				
d_{hkl}	I	d_{hkl}	I	d_{hkl}	I	Calcite 24–0027 d_{hkl} (I)	Quartz 03–0444 d_{hkl} (I)	α-Hematite 06–0502 d_{hkl} (I)	Hematite 03–0812 d_{hkl} (I)	Dolomite 34–0517 d_{hkl} (I)
				4.23	24.91		4.21 (70)			
3.84	5.09	3.83	3.93	3.83	4.97	3.852 (29)				
				3.65	0.34			3.68 (70)	3.66 (14)	
3.34	0.20	**3.34**	0.27	**3.32**	100		**3.32 (100)**			
3.03	100	3.02	100	3.02	94.31	3.03 (100)				
				2.918	0.46					2.899 (100)
2.831	1.35	2.831	2.29	2.824	1.69	2.834 (2)				
		2.686	0.11	2.688	1.60			2.69 (100)	2.69 (14)	
				2.508	1.62			2.51 (80)	2.51 (86)	
2.492	5.65	2.487	6.02	2.483	6.51	2.495 (7)				
				2.446	7.55		2.44 (40)			
2.281	9.59	2.277	9.34	2.276	13.05	2.284 (18)	2.27 (40)			
				2.230	3.49		2.22 (30)			
				2.190	0.32			2.20 (70)	2.18 (43)	
				2.120	5.74		2.12 (40)			
2.092	8.87	2.089	7.97	2.087	7.54	2.094 (27)				
1.953	0.21			1.973	2.96		1.97 (30)			
1.925	2.76	1.922	2.47	1.920	2.95	1.9261 (4)				
		1.906	9.47	1.905	10.25	1.9071 (17)				
1.874	8.45	1.872	7.06	1.869	10.10	1.8726 (34)				
				1.835	0.63		1.84 (10)	1.837 (70)	1.84 (57)	
				1.814	10.98		1.81 (80)			
1.699	0.09			1.690	0.47			1.691 (80)	1.68 (100)	
				1.669	3.33		1.67 (30)			
				1.656	1.22		1.65 (10)			
1.624	1.41	1.622	1.42	1.622	1.53	1.6259 (2)				
1.602	3.23	1.601	3.30	1.599	3.54		1.60 (10)			
1.583	0.90	1.581	0.46	1.580	0.50	1.5821 (2)			1.58 (14)	
				1.538	7.90		1.54 (90)			
1.524	2.29	1.523	1.90	1.521	2.38	1.5247 (3)				
1.505	0.97	1.503	0.77	1.501	0.94	1.5061 (**2**)				
				1.483	0.32			1.484 (70)	1.49 (14)	
1.472	0.62	1.469	0.59	1.468	0.71			1.451 (80)		

Table 4. Major- and trace-element chemistry for the reddish infill of the Albian neptunian dykes (HGas-13, 14 and 15a) and the host rock (HGas-15c). MDL – method detection level.

	MDL	HGas 13	HGas 14	HGas 15a	HGas 15c
		wt/%			
SiO_2	0.01	0.73	0.61	21.96	0.85
TiO_2	0.01	0.06	0.01	<0.01	0.02
Al_2O_3	0.01	0.24	0.22	0.17	0.28
Fe_2O_3[a]	0.04	1.12	1.45	1.91	1.62
MnO	0.01	0.08	0.08	0.06	0.08
MgO	0.01	0.50	0.58	0.45	0.62
CaO	0.01	53.65	53.41	41.25	53.17
Na_2O	0.01	0.04	0.02	0.01	0.02
K_2O	0.01	0.02	0.02	0.02	0.01
P_2O_5	0.01	0.26	0.26	0.20	0.42
Cr_2O_3	0.002	<0.002	0.002	0.003	<0.002
LOI[b]	−5.1	43.3	43.3	33.9	42.8
Total	0.01	99.95	99.94	99.96	99.94
TOT/C	0.02	12.13	12.33	9.22	12.10
TOT/S	0.02	0.03	0.03	0.03	0.03
		ppm			
Ba	1	20	13	12	13
Co	0.2	1.6	1.6	1.9	3.7
Cs	0.1	<0.1	<0.1	<0.1	<0.1
Ga	0.5	<0.5	<0.5	<0.5	<0.5
Hf	0.1	<0.1	<0.1	<0.1	<0.1
Nb	0.1	0.6	<0.1	0.1	0.3
Ni	0.1	6.7	9.3	8.1	19.3
Rb	0.1	1.3	0.5	0.3	0.3
Sc	1	<1	<1	<1	<1
Sr	0.5	199.2	209.6	169.8	221.2
Ta	0.1	<0.1	<0.1	<0.1	<0.1
Th	0.2	0.4	0.4	0.2	0.6
U	0.1	2.5	2.5	2.0	2.9

	MDL	HGas 13	HGas 14	HGas 15a	HGas 15c
		ppm			
V	8	43	39	35	67
W	0.5	0.6	0.9	2.4	1.5
Zr	0.1	2.7	2.5	2.2	3.8
Bi	0.1	<0.1	<0.1	<0.1	<0.1
Mo	0.1	0.4	0.4	0.5	0.5
Cu	0.1	2.4	2.1	3.0	10.1
Pb	0.1	1.2	1.2	1.4	1.3
Zn	1	10	12	8	14
As	0.5	3.5	4.6	4.1	9.1
Cd	0.1	0.2	0.3	0.1	0.3
Sb	0.1	0.2	0.3	0.5	0.5
Ag	0.1	<0.1	<0.1	<0.1	<0.1
Hg	0.01	0.02	<0.01	<0.01	0.01
Au(ppb)	0.5	1.9	1.5	0.5	1.0
La	0.1	9.1	8.4	6.6	10.2
Ce	0.1	4.9	4.7	4.1	6.9
Pr	0.02	1.34	1.42	0.95	1.82
Nd	0.3	5.4	5.5	4.5	7.7
Sm	0.05	1.36	1.06	0.82	1.53
Eu	0.02	0.29	0.26	0.19	0.40
Gd	0.05	1.40	1.42	0.91	1.87
Tb	0.01	0.21	0.20	0.14	0.28
Dy	0.05	1.12	1.19	0.93	1.50
Y	0.1	11.9	11.2	7.6	13.7
Ho	0.02	0.26	0.24	0.20	0.34
Er	0.03	0.66	0.71	0.48	0.80
Tm	0.01	0.10	0.08	0.07	0.11
Yb	0.05	0.40	0.50	0.36	0.62
Lu	0.01	0.09	0.07	0.05	0.09

[a]Total iron as Fe_2O_3; [b]LOI: loss on ignition

Table 5. Elemental ratios and anomalies of the samples studied.

	Σ REE	P (ppm)	$(Nd/Yb)_{SN}$	Ce/Ce∗	Pr/Pr∗	La_N/Sm_N	Y/Ho	Ti/Al
HGas -15c	34.2	917	1.13	0.34	1.30	0.97	40.3	0.17
HGas -13	26.6	567	1.12	0.29	1.32	0.97	45.8	0.6
HGas -14	25.8	567	0.91	0.30	1.45	1.15	46.7	<0.1
HGas- 15a	20.3	437	1.04	0.33	1.17	1.18	38.0	0.17

$Ce/Ce* = Ce_{SN}/(La_{SN})^{0.667} + (Nd_{SN})^{0.333}$, where SN represents normalization of Ce, La and Nd to PASS using the data $(Gd/Gd*) = 2(Gd/Gd_{shale})/(Eu/Eu_{shale} + Tb/Tb_{shale})$ and shale is Post-Archean Australian Shales (PAAS)

Landing & Lewis, 1994). It indicates the oxidation of Ce^{3+} to the strongly insoluble Ce^{4+} under oxic to suboxic redox conditions in the open ocean (e.g. Piper & Bau, 2013). The Ce ions are fractionated from each other by their complexation with CO_3^{2-} and HPO_4^{2-} and adsorb on the surfaces of suspended particles (Byrne & Kim, 1990; Sholkowitz, Shaw & Schneider, 1992; Luo & Byrne, 2004). The reaction in seawater could be bacterially mediated, especially during warmer periods (Moffett, 1990, 1994). However, in strictly inorganic solutions, the Ce anomaly occurs due to oxidative scavenging on fresh Mn-oxide surfaces (De Carlo, Wen & Irving, 1998). Fractionation of Ce ions in seawater is also related to the depth; the Ce anomaly in seawater becomes increasingly more negative from the surface to abyssal depths, as documented both in ancient sediments (e.g. Jarvis, 1984; Mazumdar *et al.* 2004) and modern environments (Piper & Bau, 2013).

The Ce/Ce* values of the material from the neptunian dykes ranged from 0.28 to 0.32 (Table 5), which is typical of oceanic seawater (e.g. Elderfield & Greaves, 1982; Wang, Liu & Schmitt, 1986; Piepgrass & Jacobsen, 1992; Piper & Bau, 2013). Similar values were obtained from the lower Turonian limestones (Scaglia Bianca) of a deep carbonate platform in the Umbria–Marche Basin (Hu, Cheng & Ji, 2009), deposited under a low accumulation rate. With La_N/Sm_N ratios of 0.97–1.18 (Table 5) the material studied did not have similar Ce anomaly values, which indicates that diagenesis had no effect on the Ce anomaly.

5.b.3. Y/Ho ratio

The Y/Ho ratio is considered an indicator of Y fractionation and the relative continental influence on the REE content of carbonate sediments. Ho belongs to the third

https://doi.org/10.1017/S0016756815001132 Published online by Cambridge University Press

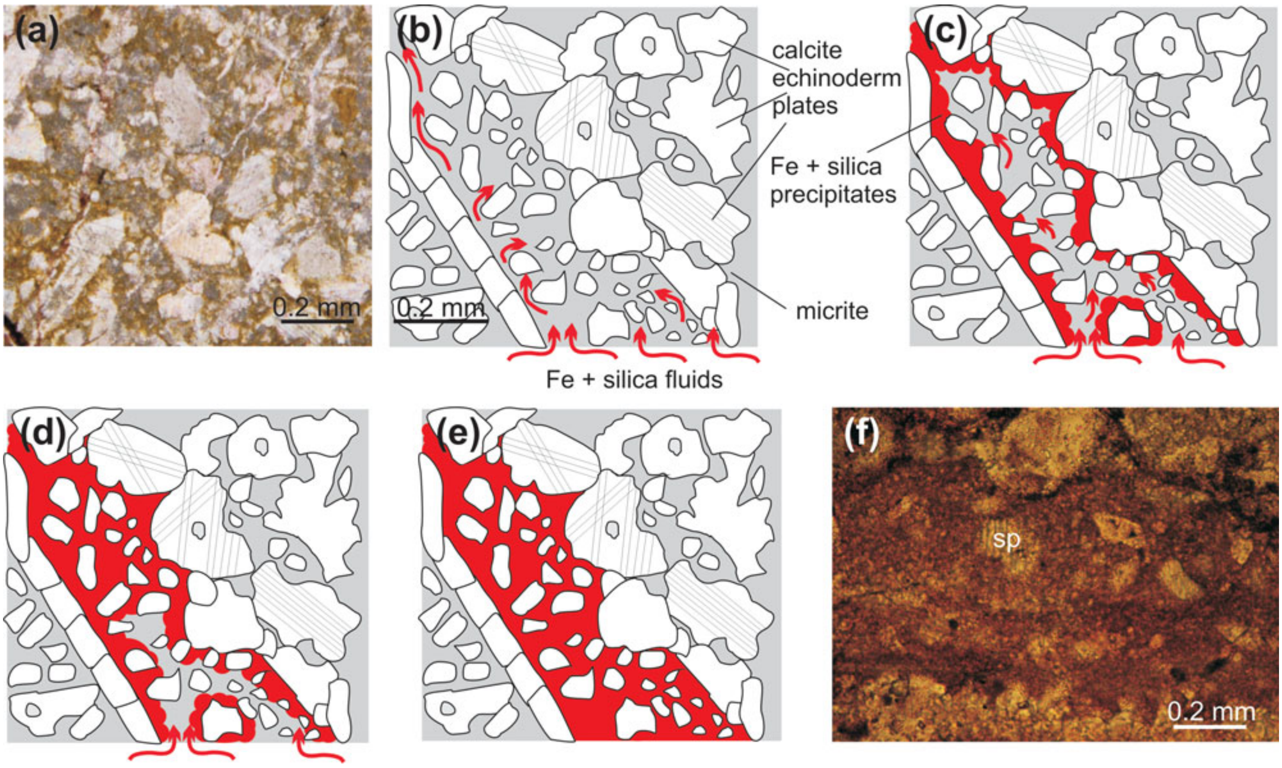

Figure 8. (Colour online) Successive steps of dyke propagation in biomicrite-type host rock. (a) Photomicrograph of biomicrite host rock before formation of the fractures and dykes. (b) The first step of dyke formation, where Fe- and silica-bearing fluids removed micrite at the contact with sparitic grains. (c) The precipitation of Fe and silica coatings formed on sparitic grains after micrite removing. (d, e) The successive precipitation of Fe and silica precipitates in a space after micrite when fluids are still active; sparitic grains left after dissolution of micrite. (f) Photomicrograph of vein completely filled with Fe and silica precipitates; sparitic grains (sp) are the only remnants after original biomicrite.

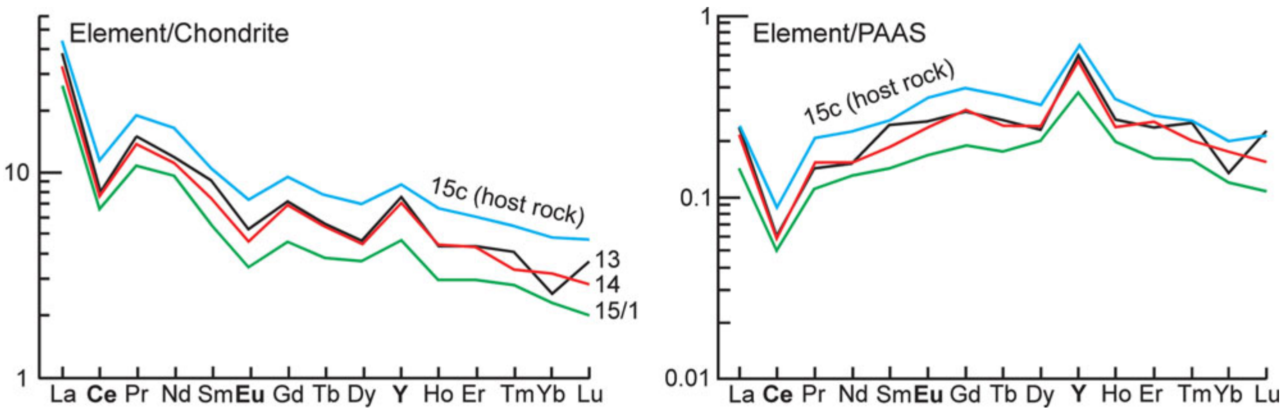

Figure 9. (Colour online) REE curves of host carbonate rock and three neptunian dykes with their immediate surroundings, normalized to chondrites (McDonough & Sun, 1995) and Post-Archean Australian Shale standards (Taylor & McLennan, 1985; McLennan, 2001).

tetrad and behaves coherently, whereas Y fractionates from them in marine reaction systems. The carbonates, which are free from terrigenous components, displayed values from 44 to 74 (Kawabe, Kitahara & Naito, 1991; Bau, 1996; Nothdurft, Webb & Kamber, 2004). In the samples studied the Y/Ho ratio was high (38.0–46.7; Table 5), close to the values of seawater.

In summary, the low REE content and chondrite- and PAAS-normalized REE + Y patterns with a negative Ce anomaly and high Y/Ho ratio indicate the authigenic removal of REEs from the water column and early diagenesis. There is a lack of data suggesting terrigenous or hydrothermal REE sources for the infilling material (e.g. Piper, 1974*a*, *b*; Palmer, 1985; Bąk, 2007).

5.c. Possible hydrothermal source of Fe and silica

5.c.1. Geochemical indices

The most characteristic feature of the material filling the dykes is the presence of hematite as aggregates or single microcrystals, which are associated with low crystalline silica or microcrystalline quartz. They create encrustations along all dyke walls.

https://doi.org/10.1017/S0016756815001132 Published online by Cambridge University Press

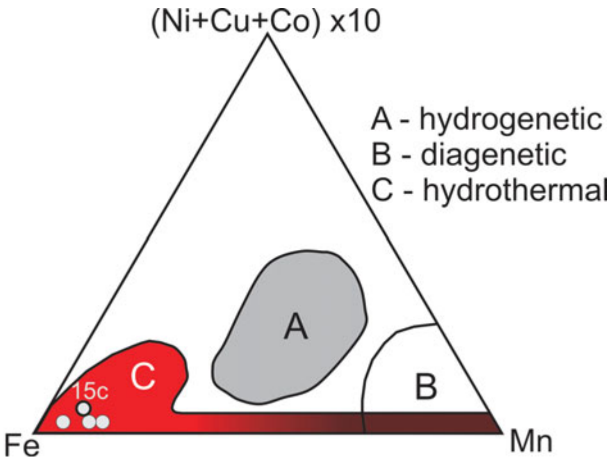

Figure 10. (Colour online) Partial bulk chemical compositions of Fe–Mn encrustations of neptunian dykes (circles) and host rock (HGas-15c) plotted on conventional ternary diagram from Bonatti, Kraemer & Ryde (1972) and Bonatti *et al*. (1976).

The formation of hematite in the dykes could be related to the fluid transportation of iron as $FeCl_3$ together with silica gel and the precipitation of iron hydroxide and later hematite (Fe_2O_3), according to the reaction: $2FeCl_3 + 3H_2O \rightarrow Fe_2O_3 + 6\ HCl$. At low pH, the precipitation of silica can be achieved because the iron hydroxide will adsorb greater quantities of silicic acid (Harder, 1964). This process could additionally be responsible for dissolution of calcium carbonate (according to reaction $CaCO_3 + 2HCl \rightarrow CaCl_2 + CO_2 + H_2O$), suggested earlier based on microfacies analysis. Hematite from ferric chloride media precipitates at temperatures below 100 °C (Riveros & Dutrizac, 1997; Liu *et al*. 2006). This would suggest that a low-temperature hydrothermal solution is the carrier of Fe ions.

The possibility of a hydrothermal origin of the Fe and Si encrustations is supported here by the chemical composition of the dykes, that is, very low concentrations of Ti (Table 5) and transition elements, and their position in the hydrothermal-origin region of the Mn–Fe–(Co + Ni + Cu)x10 ternary diagram (Fig. 10).

Fe and Si enrichments are known to originate from hydrothermal vents including mid-ocean ridge settings, intraplate submarine volcanoes, continental margins and island arcs (e.g. Alt, 1988; Hekinian *et al*. 1993; Fortin, Ferris & Scott, 1998; Kennedy, Scott & Ferris, 2003; Dekov *et al*. 2010; Zeng *et al*. 2012). They also occur as components of hydrothermal vents in shallow-water environments in close proximity to submarine volcanic activity (e.g. Tarasov *et al*. 1990, 2005; Fitzsimons *et al*. 1997; Dando, Stüben & Varnavas, 1999; Pichler, Veizer & Hall, 1999; Savelli, Marani & Gamberi, 1999; Prol-Ledesma *et al*. 2004).

5.c.2. Palaeoenvironmental indices

We propose that the Fe and Si enrichments in the neptunian dykes studied could be related to the migration of hydrothermal fluids connected with submarine volcanic activity at a neighbouring basin, which took place during middle Albian time. Such activity occurred during Aptian – late Albian time in the Zliechov Basin (Fig. 11), an adjacent sedimentary area for the Tatric Ridge. The volcanic activity was documented by the K–Ar radiometric ages of basalts occurring as veins in the Middle Triassic dolomites of the Križna Nappe (116.2 ± 6.5 Ma and 106.2 ± 1.7 Ma; Saltin Mountain and Salatinka Mountain in the Nizke Tatra Mountains: Bujnovský, Kantor & Vozäft, 1981), which were accompanied by volcanoclastics. Similar radiometric data came from alkali lamprophyre veins crossing the granitoids, which directly underlay the sedimentary strata in the same area (100.7 ± 3.8 Ma and 102.6 ± 3.8 Ma; Liptovska Dubrava in the Nizke Tatra Mountains; Spišiak & Balogh, 2002) (Fig. 11).

The radiometric ages of basalts with volcanoclastics (Križna Nappe; Nizke Tatry Mountains) were confirmed by palaeontological studies (summary in Bujnovský, Kantor & Vozäft, 1981). The youngest volcanic episode was recorded there within carbonate sediments, which contained stratigraphically important planktonic foraminiferal species *Ticinella roberti* (Gandolfi) and *Thalmannammina ticinensis* Gandolfi. Both species are found in upper Albian volcanoclastic rocks, based on the correlation of the foraminiferal zonation with other biozonations and chronostratigraphy (Gale *et al*. 2011).

The volcanic and hydrothermal activities were linked to extensional faults (Fig. 11) during Triassic – middle Cretaceous times, documented by the occasional occurrences of limestone breccia in the Zliechov Basin (Michalík, 2007). The exhalative hydrothermal vents along such extensional faults with accumulated Fe–Mn crusts occurred here much earlier during Toarcian time (Jach & Dudek, 2005). The age and palaeogeographic position of volcanic activity in the Zliechov Basin and their chemical composition is similar to other Lower Cretaceous alkaline basalts occurring in the Outer (Silesian Nappe) and Central Western Carpathians, including the Tatric Ridge (Madzin, Sýkora & Soták, 2014), and also in the Eastern Alps, Eastern Carpathians and Pannonian Basin (summary in Spišiak *et al*. 2011). This alkaline volcanism coincided with an extensional/rifting tectonic regime that finally led to the opening of the Penninic oceanic rift arms (Froitzheim, Plašienka & Schuster, 2008; Prokešová, Plašienka & Milovský, 2012). The extensional character of the faults with hydrothermal vents lasted until late Albian time in the Zliechov Basin and its surroundings. Iron hydroxides of that age, in the form of covers, coatings and fillings, are present inside upper Albian stromatolites and the underlying echinoderm-foraminiferal limestone within the Tatric sediments (Bąk *et al*. 2015). The extensional regime in the Zliechov Basin and the Tatric Ridge could be related to the initiation of a convergent zone along the Fatric–Veporic margin (Fig. 11), where the Zliechov basement (crust of the Fatric Nappe) was thrust underneath the North Veporic orogenic wedge (Plašienka, 1997), and the pelagic

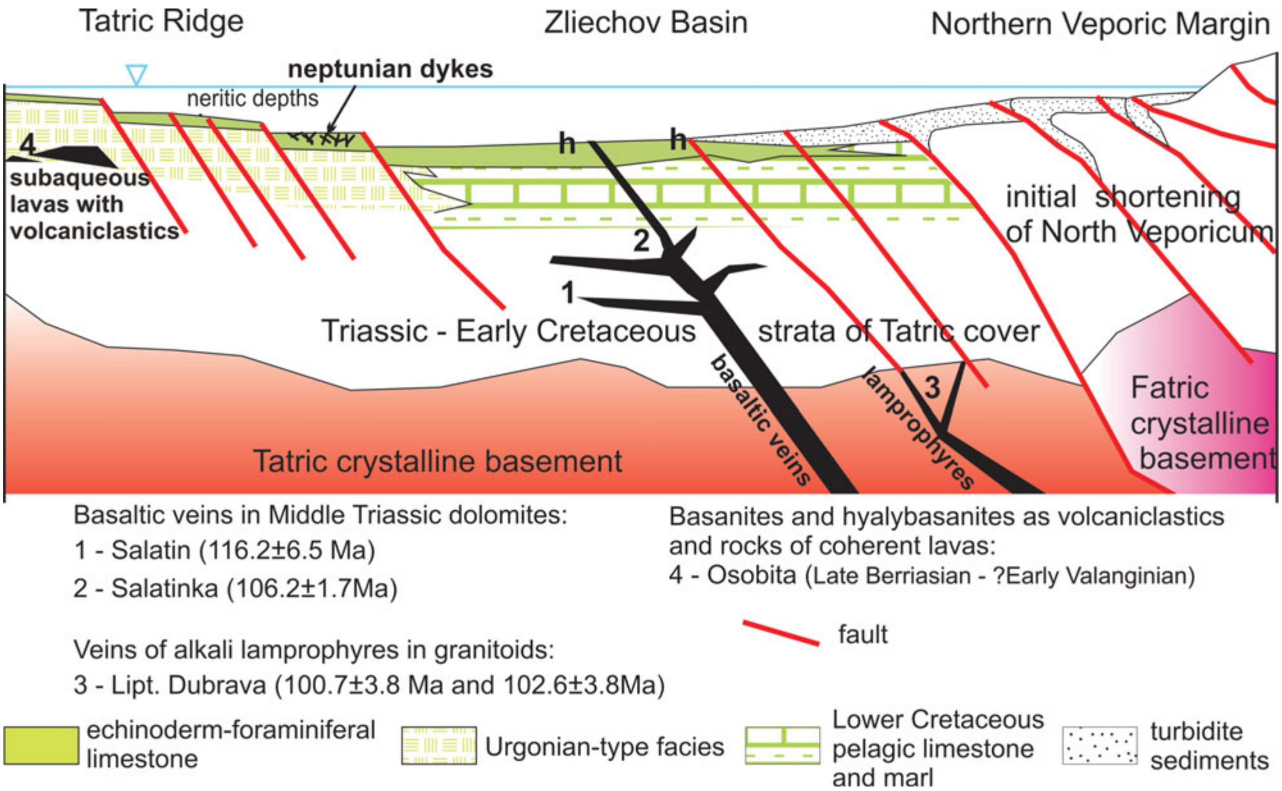

Figure 11. (Colour online) Schematic middle Albian cross-section displaying position of suspended hydrothermal activity near the Tatric Ridge, related to magmatic and volcanic processes in the surroundings. Interpretation based on data from the Tatra Mountains (Madzin, Sýkora & Soták, 2014) and the Križna Nappe (Bujnovský, Kantor & Vozäft, 1981; Spišiak & Balogh, 2002); geology after Michalík (2007) and Prokešová, Plašienka & Milovský (2012).

sedimentation in the Zliechov Basin and the Tatric area was gradually replaced by fine-grained turbidites of the Poruba Formation and the Pisana Member of the Zabijak Formation; the latter type of sedimentation occurred at greater depths. On the Tatric Ridge, an increasing depth began to form starting during middle Albian time when the seafloor was generally within the epipelagic zone (Masse & Uchman, 1997). During late Albian time, the bottom deepened to the mesopelagic zone (Bąk, 2015) and remained at that depth during the entire Cenomanian Age with gradual continued deepening.

6. Conclusions

Initiation of orogenic processes along the North Veporic orogenic wedge during early–middle Albian time (Central Western Carpathians) caused extensional deformation of sedimentary strata and their crystalline basements in the Zliechov Basin and Tatric Ridge (Michalík, 2007; Plašienka, 1997). The extensional character of these deformations led to volcanic activity in the Zliechov Basin (Bujnovský, Kantor & Vozäft, 1981; Spišiak *et al*. 2011), which could be associated with hydrothermal vents. In our interpretation, the iron and silica fluids from such vents migrated to the submerged Tatric Ridge; in the mesopelagic zone, the deepest part of this submerged ridge was characterized by carbonate sedimentation. In the areas that underwent extensional fracturing, fissures opening in the solid middle Albian carbonate substrate were filled with iron oxyhydroxides, amorphous silica and various clasts derived both from overlying sediment and, due to the leaching of micrite from the host limestone, inside the dykes. The microfacies study and chemical data of the filling in the neptunian dykes confirmed an absence of terrigenous components inside the dykes. The REE signatures from the reddish fillings suggested their authigenic removal from the water column. Taking into account the hydrothermal–hydrogenetic source of filling material in the dykes studied, we predict that further study of other dykes in the Albian Tatric sediments will result in the discovery of similar filling origins, which have been regarded so far as recrystallization products of emergence and karstification.

Acknowledgements. The study was supported by the National Science Centre, Poland to KB (grant 2011/01/B/ST10/07405) and the Ministry of Science and Higher Education to MB (Project DS-AGH University of Science and Technology, WGGiOŚ-KGOiG No. 11.11.140.173) and LNN (WGGiOŚ-KMPiG No. 11.11.140.139). We would like to thank two anonymous reviewers and the journal editor Phil Leat for constructive comments and suggestions.

Declaration of interest

None

References

ALT, J. C. 1988. Hydrothermal oxide and nontronite deposits on seamounts in the eastern Pacific. *Marine Geology* **81**, 227–39.

ANDRUSOV, D. 1968. *Grundriss der Tektonik der Nördlichen Karpaten*. SAV, Bratislava, 188 pp.

ARNAUD-VANNEAU, A., ARNAUD, H., BOISSEAU, T., DARSAC, C., THIEULOY, J. P. & VIEBAN, F. 1982. Synchronisme des crises biologiques et paléogéographiques dans le Crétacé inférieur du S.E. *de la France: un outil pour les corrélations plate-forme-bassin*. *Géologie Méditerranéenne* **9**, 153–65.

ARNAUD-VANNEAU, A., ARNAUD, H., CHAROLLAIS, J., CONRAD, M. A., COTILLON, P., FERRY, S., MASSE, J.-P. & PEYBERNES, B. 1979. Paléogéographie des calcaires urgoniens du Sud de la France. *Geobios Mémoire Spécial* **3**, 363–83.

ASCOLI, P. 1976. Foraminiferal and ostracod biostratigraphy of the Mesozoic–Cenozoic, Scotian-Shelf, Atlantic Canada. *Maritime Sediments*, Special Publication **1**, 653–771.

BABINOT, J.-F., BARBAROUX, L., TRONCHETTI, G., PHILIP, J., CANEROT, J., KOUYOUMONTZAKIS, G. & REDONDO, C. 1991. Les paléoenvironnements margino-littoraux de la plate-forme albo-cénomanienne du Bas-Aragon (Ibérides septentrionales), Espagne. *Bulletin de la Société Géologique de France* **162**, 753–62.

BĄK, K. 2007. Organic-rich and manganese sedimentation during the Cenomanian-Turonian boundary event in the Outer Carpathian Basin, a new record from the Skole Nappe, Poland. *Palaeogeography, Palaeoclimatology, Palaeoecology* **256**, 21–46.

BĄK, K. 2015. Late Albian Foraminifera from record of carbonate platform drowning on the Tatric Ridge, a part of the Carpathian domain: stratigraphic and palaeoenvironmental inferences. *Carpathian Journal of Earth and Environmental Sciences*, **10**(4), 237–50.

BĄK, K. & BĄK, M. 2013. Late Albian through Cenomanian foraminiferal assemblage from the youngest deposits of Tatra Mountains, Central Western Carpathians; biostratigraphical and palaeoecological aspects. *Acta Geologica Polonica* **63**, 223–37.

BĄK, M., BĄK, K., GÓRNY, Z. & STOŻEK, B. 2015. Evidence of bacteriogenic iron and manganese oxyhydroxides in Albian–Cenomanian marine sediments of the Carpathian realm (Poland). *Annales Societatis Geologorum Poloniae* **85**, 371–85.

BAU, M. 1996. Controls on the fractionation of isovalent trace elements in magmatic and aqueous systems: Evidence from Y/Ho, Zr/Hf, and lanthanide tetrad effect. *Contributions to Mineralogy and Petrology* **123**, 323–33.

BELLANCA, A., MASETTI, D. & NERI, R. 1997. Rare earth elements in limestone/marlstone couplets from the Albian-Cenomanian Cismon section (Venetian region, northern Italy): assessing REE sensitivity to environmental changes. *Chemical Geology* **141**, 141–52.

BERTRAM, C. J. & ELDERFIELD, H. 1993. The geochemical balance of the rare earth elements and neodymium isotopes in the oceans. *Geochimica et Cosmochimica Acta* **57**, 1957–86.

BONATTI, E., KRAEMER, T. & RYDE, U. H. 1972. Classification and genesis of Fe-Mn deposits. In *Ferromanganese Deposits on the Ocean Floor* (ed. D. R. Horn), pp. 149–65. New York: Arden House.

BONATTI, E., ZERBI, M., KAY, R. & RYDELL, H. S. 1976. Metalliferous deposits from the Apennine ophiolites: Mesozoic equivalents of modern deposits from oceanic spreading centre. *Geological Society of America Bulletin* **87**, 83–94.

BRYNDAL, T. 2014. *Identification of small catchments prone to flash flood generation in the Polish Carpathians*. Kraków: Wydawnictwo Naukowe Uniwersytetu Pedagogicznego. Prace Monograficzne Uniwersytetu Pedagogicznego, 690, 180 pp.

BUJNOVSKÝ, A., KANTOR, J. & VOZÄFT, J. 1981. Radiometric dating of Mesozoic basic eruptive rocks of the Krížna Nappe in the NW part of the Low Tatra. *Geologica Carpathica* **32**, 221–30.

BYRNE, R. H. & KIM, K. H. 1990. Rare earth element scavenging in seawater. *Geochimica et Cosmochimica Acta* **54**, 2645–56.

CARON, M. 1985. Cretaceous planktonic foraminifera. In *Plankton Stratigraphy* (eds H. M. Bolli, J. B. Saunders & K. Perch-Nielsen), pp. 17–86. Cambridge: Cambridge University Press.

DANDO, P. R., STÜBEN, D. & VARNAVAS, S. P. 1999. Hydrothermalism in the Mediterranean Sea. *Progress in Oceanography* **44**, 333–67.

DE BAAR, H. J. W., BACON, M. P. & BREWER, P. G. 1985. Rare earth elements in the Pacific and Atlantic oceans. *Geochimica et Cosmochimica Acta* **49**, 1943–59.

DE CARLO, E. H., WEN, X.-Y. & IRVING, M. 1998. The influence of redox reactions on the uptake of dissolved Ce by suspended Fe and Mn oxide particles. *Aquatic Geochemistry* **3**, 357–89.

DEKOV, V. M., PETERSEN, S., GARBE-SCHONBERG, C. D., KAMENOV, G. D., PERNER, M., KUZMANN, E. & SCHMIDT, M. 2010. Fe-Si-oxyhydroxide deposits at a slow spreading centre with thickened oceanic crust: the Lilliput hydrothermal field (9°33′S, Mid-Atlantic Ridge). *Chemical Geology* **278**, 186–200.

ELDERFIELD, H. & GREAVES, M. J. 1982. The rare earth elements in seawater. *Nature* **96**, 58214–9.

FITZSIMONS, M. F., DANDO, P. R., HUGHES, J. A., THIERMANN, F., AKOUMIANAKI, I. & PRATT, S. M. 1997. Submarine hydrothermal brine seeps off Milos, Greece: observations and geochemistry. *Marine Chemistry* **57**, 325–40.

FORTIN, D., FERRIS, F. G. & SCOTT, S. D. 1998. Formation of Fe-silicates and Fe-oxides on bacterial surfaces in samples collected near hydrothermal vents on the Southern Explorer Ridge in the northeast Pacific Ocean. *American Mineralogist* **83**, 1399–408.

FROITZHEIM, N., PLAŠIENKA, D. & SCHUSTER, R. 2008. Alpine tectonics of the Alps and Western Carpathians. In *The Geology of Central Europe. Vol. 2: Mesozoic and Cenozoic* (ed. T. McCann), pp. 1141–232. London: Geological Society's Publishing House.

GALE, A., BOWN, P., CARON, M., CRAMPTON, J., CROWHURST, S. J., KENNEDY, W. J., PETRIZZO, M. R. & WRAY, D. S. 2011. The uppermost Middle and Upper Albian succession at the Col de Palluel, Hautes-Alpes, France: An integrated study (ammonites, inoceramid bivalves, planktonic foraminifera, nannofossils geochemistry, stable oxygen and carbon isotopes, cyclostratigraphy). *Cretaceous Research* **32**, 59–130.

GERMAN, C. R. & ELDERFIELD, H. 1990. Rare earth elements in the NW Indian Ocean. *Geochimica et Cosmochimica Acta* **54**, 1929–40.

GRABOWSKI, J. 1997. Paleomagnetic results from the cover (High Tatric) unit and nummulitic Eocene in the Tatra Mts (Central West Carpathians, Poland) and their tectonic implications. *Annales Societatis Geologorum Poloniae* **67**, 13–23.

https://doi.org/10.1017/S0016756815001132 Published online by Cambridge University Press

GREAVES, M. J., ELDERFIELD, H. & SHOLKOVITZ, E. R. 1999. Aeolian sources of rare earth elements to the Western Pacific Ocean. *Marine Chemistry* **68**, 31–8.

GUZIK, K. & JACZYNOWSKA, W. (eds) 1978. *Geological Map of the Tatra Mountains, scale 1:10,000: Kościelec Sheet (B4)*. Warszawa: Wydawnictwa Geologiczne.

HALEY, B. A., KLINKHAMMER, G. P. & MIX, C. 2005. Revisiting the rare earth elements in foraminiferal tests. *Earth and Planetary Science Letters* **239**, 79–97.

HARDER, H. 1964. Können Eisensäuerlinge die Genese der Lahn-Dill-Erze erklären? *Beiträge zur Mineralogie und Petrographie* **9**, 379–422.

HEKINIAN, R., HOFFERT, M., LARQUE, P., CHEMINEE, J. L., STOFFERS, P. & BIDEAU, D. 1993. Hydrothermal Fe and Si oxyhydroxide deposits from South Pacific intraplate volcanoes and East Pacific Rise axial and off-axial regions. *Economic Geology* **88**, 2099–121.

HOLSER, W. T. 1997. Evaluation of the application of rare-earth elements to paleoceanography. *Palaeogeography, Palaeoclimatology, Palaeoecology* **132**, 309–23.

HOVORKA, D., DOSTÁL, J. & SPIŠIAK, J. 1999. Geochemistry of the Cretaceous alkali basaltic rocks of the central part of the Western Carpathians (Slovakia). *Kryštalinikum* **25**, 37–48.

HOVORKA, D. & SPIŠIAK, J. 1981. Hyalobasanites (Limburgites) of Osobitá peak in the Tatra Mts. In *Palaeovolcanism in the Western Carpathians* (eds Š. Bajaník & D. Hovorka), pp. 145–56. Bratislava: Geologicky ústav D. Štúra.

HOVORKA, D. & SPIŠIAK, J. 1988. *Mesozoic Volcanism of the Western Carpathians* (in Slovak with English summary). Bratislava: Veda, 263 pp.

HU, X., CHENG, W. & JI, J. 2009. Origin of Cretaceous oceanic Red Beds from the Vispi quarry section, visible reflectance and inorganic geochemistry. In *Cretaceous Oceanic Red Beds: Stratigraphy, Composition, Origins and Paleo-Ceanographic and Paleoclimatic Significance* (eds X. Hu, C. Wang, R. W. Scott, M. Wagreich & L. Jansa), pp. 183–97. SEPM, Tulsa, Special Publication **91**.

IVAN, P., HOVORKA, D. & MÉRES, Š. 1999. Riftogenic volcanism in the Western Carpathian geological history: a review. *GeoLines* **9**, 41–7.

JACH, R. & DUDEK, T. 2005. Origin of a Toarcian manganese carbonate/silicate deposit from the Krížna Unit, Tatra Mountains, Poland. *Chemical Geology* **224**, 136–52.

JARVIS, I. 1984. Rare earth element geochemistry of Late Cretaceous chalks and phosphorites of Northern France. In *Phosphorite* (eds G. V. Rao, S. P. Dasgupta, A. Pant & R. Choudhuri), pp. 179–90. Udaipur, Rajasthan: Geological Survey of India, Special Publication **17**.

KAMBER, B. S. & WEBB, G. E. 2001. The geochemistry of late Archaean microbial carbonate: implications for ocean chemistry and continental erosion history. *Geochimica et Cosmochimica Acta* **65**, 2509–25.

KAWABE, I., KITAHARA, Y. & NAITO, K. 1991. Non-chondritic yttrium/holmium ratio and lanthanide tetrad effect observed in pre-Cenozoic limestones. *Geochemical Journal* **25**, 31–44.

KENNEDY, C. B., SCOTT, S. D. & FERRIS, F. G. 2003. Characterization of bacteriogenic iron oxide deposits from Axial Volcano, Juan de Fuca Ridge, Northeast Pacific Ocean. *Geomicrobiology Journal* **20**, 124–99.

KOCSIS, L., TRUEMAN, C. N. & PALMER, M. R. 2010. Protracted diagenetic alteration of REE contents in fossil bioapatites: direct evidence from Lu–Hf isotope systematic. *Geochimica et Cosmochimica Acta* **74**, 6077–92.

KOEPPENKASTROP, D. & DE CARLO, E. H. 1992. Sorption of rare earth elements from seawater onto synthetic mineral particles: an experimental approach. *Chemical Geology* **95**, 251–63.

KOSCHINSKY, A. & HEIN, J. R. 2003. Uptake of elements from seawater by ferromanganese crusts: solid-phase associations and seawater speciation. *Marine Geology* **198**, 331–51.

KOTAŃSKI, Z. 1961. Tectogénèse et reconstitution de la paléogéographie de la zone haut-tatrique dans les tatras. *Acta Geologica Polonica* **11**, 187–412.

KOTAŃSKI, Z. & RADWAŃSKI, A. 1959. High-Tatric Tithonian in the Osobita region, its fauna with Pygope diphya and products of the volcanoes, Western Tatra Mts. *Acta Geologica Polonica* **9**, 519–34.

KOUTSOUKOS, E. A. M., LEARY, P. N. & HART, M. B. 1989. *Favusella* Michael (1972): evidence of ecophenotypic adaptation of a planktonic foraminifer to shallow water carbonate environments during the Mid-Cretaceous. *Journal of Foraminiferal Research* **19**, 324–36.

KRAJEWSKI, K. 1981. Pelagic stromatolites from the High-Tatric Albian limestones in the Tatra Mts. *Kwartalnik Geologiczny* **25**, 731–59.

KRAJEWSKI, K. 2003. Facies development and lithostratigraphy of the Hightatric mid-Cretaceous (Zabijak Formation) in the Polish Tatra Mountains. *Studia Geologica Polonica* **121**, 81–158.

LÉCUYER, C., REYNARD, B. & GRANDJEAN, P. 2004. Rare earth element evolution of Phanerozoic seawater recorded in biogenic apatites. *Chemical Geology* **204**, 63–102.

LEFELD, J. 1968. Stratigraphy and paleogeography of the High-Tatric Lower Cretaceous in the Tatra Mountains. *Studia Geologica Polonica* **24**, 1–115.

LEFELD, J. 1974. Middle-Upper Jurassic and Lower Cretaceous biostratigraphy and sedimentology of the Sub-Tatric Succession in the Tatra Mts (Western Carpathians). *Acta Geologica Polonica* **24**, 277–64.

LEFELD, J. 1985. Wysoka Turnia Limestone Formation. In *Jurassic and Cretaceous Lithostratigraphic Units in the Tatra Mountains* (eds J. Lefeld, A. Gaździcki, A. Iwanow, K. Krajewski & K. Wójcik), pp. 33–4. Kraków: *Studia Geologica Polonica* **84**.

LIU, W., ETSCHMANN, B., BRUGGER, J., SPICCIA, L., FORAN, G. & MCINNES, B. 2006. UV-vis spectrophotometric and XAFS studies of ferric chloride complexes in hypersaline LiCl solutions at 25–90°C. *Chemical Geology* **231**, 326–49.

LUO, Y. R. & BYRNE, R. H. 2004. Carbonate complexation of yttrium and the rare earth elements in natural waters in natural water. *Geochimica et Cosmochimica Acta* **68**, 691–9.

MADZIN, J., SÝKORA, M. & SOTÁK, J. 2014. Stratigraphic position of alkaline volcanic rocks in the autochthonous cover of the High-Tatric Unit (Western Tatra Mts, Central Western Carpathians, Slovakia). *Geological Quarterly* **58**, 163–80.

MASSE, J.-P. & UCHMAN, A. 1997. New biostratigraphic data on the Early Cretaceous platform carbonates of the Tatra Mountains, Western Carpathians, Poland. *Cretaceous Research* **18**, 713–29.

MAZUMDAR, A., TANAKA, K., TAKAHASHI, T. & KAWABE, I. 2004. Characteristics of rare earth element abundances in shallow marine continental platform carbonates of Late Neoproterozoic successions from India. *Geochemical Journal* **37**, 277–89.

McDonough, W. F. & Sun, S.-S. 1995. Composition of the Earth. *Chemical Geology* **120**, 223–53.
McLennan, S. M. 1989. Rare earth elements in sedimentary rocks; influence of provenance and sedimentary processes. *Reviews in Mineralogy* **21**, 169–200.
McLennan, S. M. 2001. Relationships between the trace element composition of sedimentary rocks and continental crust. *Geochemistry, Geophysics, Geosystems* **2**, 1–24.
Michael, F. Y. 1972. Planktonic foraminifera from the Comanchean Series (Cretaceous) of Texas. *Journal of Foraminiferal Research* **2**, 200–20.
Michalík, J. 1994. Lower Cretaceous carbonate platform facies, Western Carpathians. *Palaeogeography, Palaeoclimatology, Palaeoecology* **111**, 263–77.
Michalík, J. 2007. Sedimentary rock record and microfacies indicators of the latest Triassic to mid-Cretaceous tensional development of the Zliechov Basin (Central Western Carpathians). *Geologica Carpathica* **58**, 443–53.
Michalík, J. & Soták, J. 1990. Lower Cretaceous shallow marine buildups in the Western Carpathians and their relationship to pelagic facies. *Cretaceous Research* **11**, 211–27.
Michalík, J. & Vašíček, Z. 1989. Lower Cretaceous stratigraphy and paleogeography of the Czechoslovakian Western Carpathians. In *Cretaceous of the Western Tethys* (ed. J. Wiedmann), pp. 505–23. Proceedings of the 3rd International Cretaceous Symposium, Tübingen 1987. Stuttgart: Schweizerbart.
Mišik, M. 1990. Urgonian facies in the Western Carpathians. *Knihovna zemniho plynu a nafty* **9a**, 25–54.
Moffett, J. W. 1990. Microbially mediated cerium oxidation in seawater. *Nature* **345**, 421–3.
Moffett, J. W. 1994. A radiotracer study of cerium and manganese uptake onto suspended particles in Chesapeake Bay. *Geochimica et Cosmochimica Acta* **58**, 695–703.
Morycowa, E. & Lefeld, J. 1966. Les Madréporaires des calcaires urgoniens de la série haut-tatrique dans la Tatra Polonaise. *Rocznik Polskiego Towarzystwa Geologicznego* **36**, 519–42.
Nemčok, J., Bezák, V., Janák, M., Kahan, Š., Ryka, W., Kohút, M., Lehotský, I., Wieczorek, J., Zelman, J., Mello, J., Halouzka, R., Rączkowski, W., Kotański, Z. & Reichwalder, P. 1993. *Geological Map of Tatra Mts 1:50 000*. Bratislava: State Geological Institute of Dionýz Štúr.
Nothdurft, L. D., Webb, G. E. & Kamber, B. S. 2004. Rare earth element geochemistry of Late Devonian reefal carbonates, Canning Basin, Western Australia: confirmation of a seawater REE proxy in ancient limestones. *Geochimica et Cosmochimica Acta* **68**, 263–83.
Palmer, M. R. 1985. Rare earth elements in foraminifera tests. *Earth and Planetary Science Letters* **73**, 285–98.
Parekh, P. P., Möller, P., Dulski, P. & Bausch, W. M. 1977. Distribution of trace elements between carbonate and non-carbonate phases of limestone. *Earth and Planetary Science Letters* **34**, 39–50.
Passendorfer, E. 1930. Étude stratigraphique et paléontologique du Cretacé de la série hauttatrique darns les Tatras. *Prace Państwowego Instytutu Geologicznego* **2**, 351–676.
Passendorfer, E. 1978. *Jak powstały Tatry* (In Polish, French summary). Warszawa: Wydawnictwa Geologiczne, 305 pp.
Philip, J., Masse, J.-P. & Bessais, H. 1989. Organisation et évolution sedimentaires d'une marge de plate-forme carbonatée: l'Albien-Cénomanien de Tunisie central. *Géologie Médittteraneé* **16**, 155–69.
Picard, S., Lécuyer, C., Barrat, J.-A., Garcia, J.-P., Dromart, G. & Sheppard, S. M. F. 2002. Rare earth element contents of Jurassic fish and reptile teeth and their potential relation to seawater composition (Anglo-Paris Basin, France and England). *Chemical Geology* **186**, 1–16.
Pichler, T., Veizer, J. & Hall, G. E. M. 1999. The chemical composition of shallow-water hydrothermal fluids in Tutum Bay, Ambitle Island, Papua New Guinea and their effect on ambient seawater. *Marine Chemistry* **64**, 229–52.
Piepgras, D. J. & Jacobsen, S. B. 1992. The behavior of rare Earth elements in seawater: precise determination of variations in the North Pacific water column. *Geochimica et Cosmochimica Acta* **56**, 1851–62.
Piper, D. Z. 1974*a*. Rare earth elements in the sedimentary cycle, a summary. *Chemical Geology* **14**, 285–304.
Piper, D. Z. 1974*b*. Rare earth elements in ferromanganese nodules and other marine phases. *Geochimica et Cosmochimica Acta* **38**, 1007–22.
Piper, D. Z. 1991. Geochemistry of a Tertiary sedimentary phosphate deposit, Baja California Sur, Mexico. *Chemical Geology* **92**, 283–316.
Piper, D. Z. & Bau, M. 2013. Normalized Rare Earth Elements in water, sediments, and wine: Identifying sources and environmental redox conditions. *American Journal of Analytical Chemistry* **4**, 69–83.
Plašienka, D. 1997. Cretaceous tectonochronology of the Central Western Carpathians, Slovakia. *Geologica Carpathica* **48**, 99–111.
Plašienka, D. 1999. *Tectochronology and Paleotectonic Model of the Jurassic–Cretaceous Evolution of the Central Western Carpathians* (in Slovak with English summary). Bratislava: Veda, 128 pp.
Prokešová, R., Plašienka, D. & Milovský, R. 2012. Structural pattern and emplacement mechanisms of the Krížna cover nappe (Central Western Carpathians). *Geologica Carpathica* **63**, 13–32.
Prol-Ledesma, R. M., Canet, C., Torres-Vera, M. A., Forrest, M. J. & Armienta, M. A. 2004. Vent fluid chemistry in Bahía Concepción coastal submarine hydrothermal system, Baja California Sur, Mexico. *Journal of Volcanology and Geothermal Research* **137**, 311–28.
Rabowski, F. 1959. High-Tatric series in Western Tatra. *Prace Instytutu Geologicznego* **27**, 5–178.
Reynard, B., Lécuyer, C. & Grandjean, P. 1999. Crystal-chemical controls on rare-earth element concentrations in fossil biogenic apatites and implications for paleoenvironmental reconstructions. *Chemical Geology* **155**, 233–41.
Risch, H. 1971. Stratigraphie der höheren Unterkreide der Subbotina, N. N. 1953. Fossil Foraminifera of the USSR, bayrischen Kalkalpen mit Hilfe von Mikrofossilien, Palae- Globigerinidae, Hantkeninidae and Globorotaliidae. *Trudy Ontographica, Abt. A* **137**, 1–80.
Riveros, P. A. & Dutriyzac, J. E. 1997. The precipitation of hematite from ferric chloride media. *Hydrometallurgy* **46**, 85–104.
Roberts, N. L., Piotrowski, A. M., Elderfield, H., Eglinton, T. I. & Lomas, M. W. 2012. Rare earth element association with foraminifera. *Geochimica et Cosmochimica Acta* **94**, 57–71.
Rősier, W., Lutze, G. F. & Pflaumann, U. 1979. Some Cretaceous planktonic formaminifers (*Favusella*) of DSDP Site 397 (eastern North Atlantic). In *Proceedings of the Deep Sea Drilling Program, Scientific Results, Leg 47* (eds U. von Rad, W. B. F. Ryan, M. A. Arthur *et al.*),

https://doi.org/10.1017/S0016756815001132 Published online by Cambridge University Press

pp. 273–81. Texas A & M University, Ocean Drilling Program, College Station, TX, United States, 47, Part 1.

SAVELLI, C., MARANI, M. & GAMBERI, F. 1999. Geochemistry of metalliferous, hydrothermal deposits in the Aeolian arc Tyrrhenian Sea. *Journal of Volcanology and Geothermal Research* **88**, 305–23.

SHOLKOVITZ, E. 1988. Rare earth elements in the North Atlantic Ocean, Amazon Delta and East China Sea: reinterpretation of terrigenous input patterns to the oceans. *American Journal of Science* **288**, 236–81.

SHOLKOVITZ, E., LANDING, W. M. & LEWIS, B. L. 1994. Ocean particle chemistry: the fractionation of rare earth elements between suspended particles and seawater. *Geochimica et Cosmochimica Acta* **58**, 1576–80.

SHOLKOVITZ, E., SHAW, T. J. & SCHNEIDER, D. L. 1992. The geochemistry of rare earth elements in the seasonally anoxic water column and porewaters of Chesapeake Bay. *Geochimica et Cosmochimica Acta*, **56**, 3389–402.

SHOLKOVITZ, E. & SHEN, G. T. 1995. The incorporation of rare-earth elements in modern coral. *Geochimica et Cosmochimica Acta* **59**, 2749–56.

SPIŠIAK, J., ARVENSIS, M., LINKEŠOVÁ, M., PITOŇÁK, P. & CAŇO, F. 1991. Basanite dyke in granitoids near Dúbrava, Nízke Tatry Mts, Central Slovakia. *Mineralia Slovaca* **23**, 339–45 (in Slovak).

SPIŠIAK, J. & BALOGH, K. 2002. Mesozoic alkali lamprophyres in Variscan granitoids of Malé Karpaty and Nizke Tatry mountains - geochronology and geochemistry. *Geologica Carpathica* **53**, 295–301.

SPIŠIAK, J. & HOVORKA, D. 1997. Petrology of Western Carpathians Cretaceous primitive alkaline volcanics. *Geologica Carpathica* **48**, 113–21.

SPIŠIAK, J., PLAŠIENKA, D., BUCOVÁ, J., MIKUŠ, T. & UHER, P. 2011. Petrology and palaeotectonic setting of Cretaceous alkaline basaltic volcanism in the Pieniny Klippen Belt (Western Carpathians, Slovakia). *Geologica Carpathica* **55**, 27–48.

STANISZEWSKA, A. & CIBOROWSKI, T. 2000. Lower Cretaceous breccia from autochthonous High-Tatric Succession in Western Tatra Mts (southern Poland). *Przegląd Geologiczny* **48**, 246–50 (in Polish with English summary).

TARASOV, V. G., GEBRUK, A. V., MIRONOV, A. N. & MOSKALEV, L. I. 2005. Deep-sea and shallow-water hydrothermal vent communities: two different phenomena? *Chemical Geology* **224**, 5–39.

TARASOV, V. G., PROPP, M. V., PROPP, L. N., ZHIRMUNSKY, A. V., NAMSARAEV, B. B., GORLENKO, V. M. & STARYNIN, D. A. 1990. Shallow-water gasohydrothermal vents of Ushishir volcano and the ecosystem of Kraternaya Bight (the Kurile Islands). *Marine Ecology* **11**, 1–23.

TAYLOR, S. R. & MCLENNAN, S. M. 1985. *The Continental Crust: Its Composition and Evolution: An Examination of the Geochemical Record Preserved in Sedimentary Rocks*. Carlton: Blackwell Scientific Publication, 312 pp.

WANG, Y. L., LIU, Y.-G. & SCHMITT, R. A. 1986. Rare earth element geochemistry of South Atlantic deep sea sediments: Ce anomaly change at ~ 54 My. *Geochimica et Cosmochimica Acta* **50**, 1337–55.

WEBB, G. E. & KAMBER, B. S. 2000. Rare earth elements in Holocene reefal microbialites: A new shallow seawater proxy. *Geochimica et Cosmochimica Acta* **64**, 1557–65.

ZENG, Z., OUYANG, H., YIN, X., CHEN, S., WANG, X. & WU, L. 2012. Formation of Fe–Si–Mn oxyhydroxides at the PACMANUS hydrothermal field, Eastern Manus Basin: Mineralogical and geochemical evidence. *Journal of Asian Earth Sciences* **60**, 130–46.